Supercapacitor Applications of Pure and Cerium doped Nickel Oxide

Dissertation Submitted to the

University of Kerala for the Partial Fulfilment of the Requirement

for the Award of The Degree of

MASTER OF SCIENCE

In

PHYSICS

2020-2022

Contents

LIST OF FIGURES

LIST OF TABLES

Abstract

The need for developing efficient and affordable energy storage technologies increased since the energy obtaining from these renewable energy sources is less compared to those from fossil fuels. Hence studies regarding efficient materials for the fabrication of supercapacitors are of great interest. Since energy storage is the leading solution for the fast growing energy crisis, in this work supercapacitor applications of NiO and Ce doped NiO are investigated. Nanoparticles are synthesized by modified auto combustion method and the structural confirmation is done using XRD analysis. Morphological and elemental analysis are done using FE-SEM and EDAX spectra. Absorption properties are studied and bandgap was evaluated using UV-Visible spectroscopy. Characteristic vibrational modes are investigated using Raman and FTIR spectra. Cyclic voltammetry measurements at different scan rates and Galvanostatic charge discharge measurements at different current densities are performed to probe the electrochemical response which revealed the potential of Ce doped NiO as an electrode material for energy storage devices.

CHAPTER 1

INTRODUCTION

Issues relating to energy are among the most important and difficult challenges confronting the world today. Providing sufficient energy to meet the requirements of a growing world population with rising living standards will require major advances in energy supply and efficiency. Consequently, our scientific research is being directed to the development of more energy sources apart from the existing conventional energy sources. Till date, fossil fuels including coal, oil, and natural gas have been the primary sources of energy. They are available in finite quantities only. As we keep extracting them, they will run out sooner or later. In the recent decades, renewable sources of energy such as sunlight, wind, tides, waves, thermal energy stored in the earth's crust-have the benefit of being available in one form or another nearly everywhere, have gathered much attention[1]. The need for developing efficient and affordable energy storage technologies increased since the energy obtaining from these renewable energy sources is less compared to those from fossil fuels. Thus, significant efforts have been made in developing new technologies and energy storage systems. Electrochemical energy storage systems constitute an essential element in the development of sustainable energy technologies.

1.1 Energy Storage Devices

Our energy consumption, coupled with diminishing fossil fuel resources and their effect on the health of the environment are the main causes of the world energy crisis. The effects of the energy crisis are both environmental and economic. Energy storage is the leading solution for the fast growing energy crisis.

1.1.1 Batteries

Batteries are energy storage devices which store energy in chemical form and transfer it in electrical form. There are two basic types of batteries: primary and secondary. Primary batteries are single use batteries because they cannot be recharged. Examples include: alkaline, zinc, carbon, silver oxide and some lithium metal batteries. Secondary batteries are rechargeable. The batteries found in smartphones, electronic tablets and automobiles are secondary batteries. Examples include: nickel-cadmium, lead-acid, nickel-metal hydride and lithium-ion batteries [2]. Low energy efficiency, limited power capability, and waste battery

disposal are some of the limitations of secondary battery. Fig. 1.1 shows the schematic diagram of a lithium-ion battery.

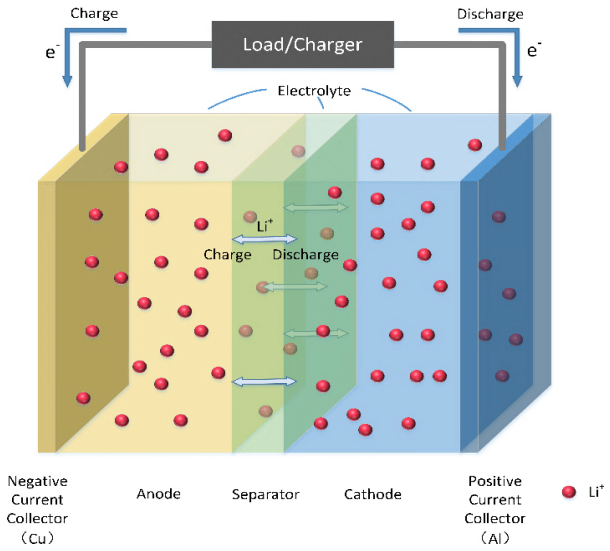

Fig. 1.1: Schematic representation of a Lithium-ion battery.

1.1.2 Fuel Cells

A fuel cell is an electrochemical device that converts chemical energy into electrical energy. They are similar to batteries but require a continuous source of fuel, such as hydrogen, natural gas or methanol. Their size ranges from hand-held systems to megawatt power stations. Large fuel cells operate at high temperatures while proton-exchange membrane fuel cell operate at low temperatures. Fuel cells continue to produce electricity as long as fuel is available. Hydrogen fuel cells are used to supply power for satellites, boats and submarines. Fig. 1.2 represents a proton-exchange membrane fuel cell.

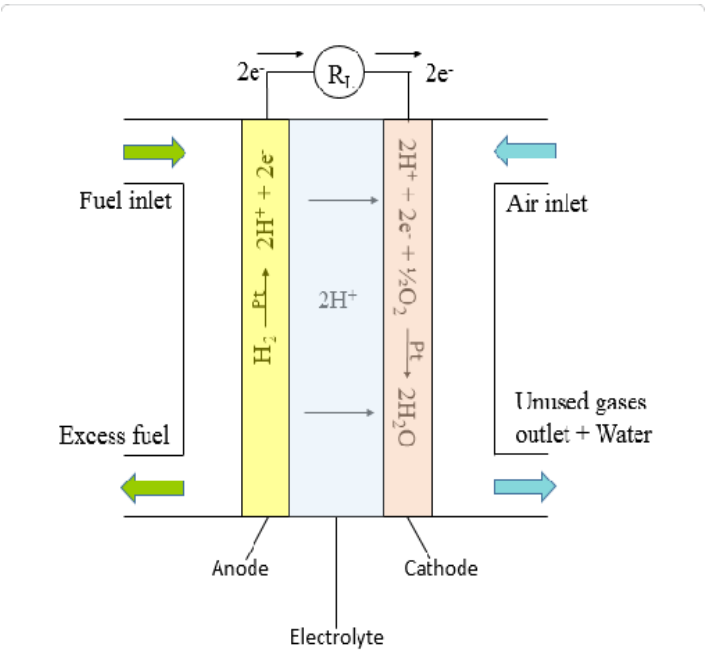

Fig. 1.2: Representation of a proton-exchange membrane fuel cell.

1.1.3 Capacitors

Capacitor is an electrochemical device that stores energy in the form of electrical charge. A capacitor consists of two conducting plates separated by an insulating material called the dielectric. The capacitance is the amount of electric charge stored in the capacitor at 1 Volt. Capacitance is directly proportional to the surface area of plates and is inversely proportional to the separation between the plates. It also depends on the dielectric constant of the substance between the plates.

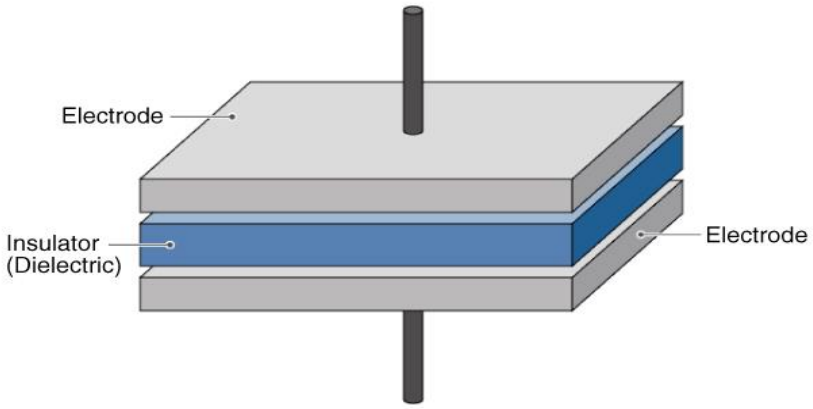

Fig. 1.3: Basic structure of a capacitor

1.1.4 Super capacitors

Supercapacitors are electrochemical energy storage devices which are used to store extremely large amount of electrical charge. They do not require fuel to operate. They are also known as double-layer capacitors or ultracapacitors. Super capacitor offers very high capacitance in a small package unlike regular capacitors. Super capacitor has very high power density and low internal resistance, which makes them able to store and deliver energy at higher rates than the battery.

1.2 Comparison between Battery, Fuel cell, Capacitor and Supercapacitor

The main difference between fuel cell and battery is that a fuel cell can supply electrical energy for a long period of time compared to a normal battery. A fuel cell receives fuel and oxygen from an external source on a continuous basis, allowing it to operate for an extended period of time; however, a battery contains a finite amount of fuel and oxidant, and these two components degrade over time, limiting its ability to supply electrical energy for an extended period of time. Fuel cells can store a high quantity of energy but have a lower power density. Supercapacitors, on the other hand, can deliver a large quantity of power in a short period of time. Conventional capacitors store energy physically as positive and negative charges on two parallel conductive plates, which offers a high power density but a low energy density. The super capacitor offers a higher power density than most batteries and higher energy density than capacitors. The basic characteristics of batteries, fuel cells, capacitors and supercapacitors are compared in table 1.1.

Table 1.1: Comparison of batteries, fuel cells, capacitors and supercapacitors

Property	Batteries	Fuel cells	Capacitors	Supercapacitors
Charge/Discharge time	1 to 10 h	Typically 10-300 h.	Picoseconds to Milliseconds	Milliseconds to seconds
Operating Temperature	-20 to +65ºC	+25 to +90ºC	-20 to +90ºC	-40 to +85ºC

Operating voltage	1.25 to 4.2 V/cell	0.6 V/cell	6 to 800V	2.3V to 2.75 V/cell
Power Density	0.005 to 0.4 kW/kg	0.001 to 0.1 kW/kg	0.25 to 10,000 kW/kg	10 to 100 kW/kg
Life	150 to 1500 cycles	1500-10000 h	>100,000 cycles	30,000+hrs average
Weight	1g to10kg	20g to 5kg	1g to 10kg	1g to 2g
Energy Density	8 to 600Wh/kg	300 to 3000Wh/kg	0.01 to 0.05Wh/kg	1 to 5Wh/kg
Capacitance	N/A	N/A	10pF to 2.2mF	100mF to >2F

Super capacitor is capable to store high energy density with ultra high power density that bridge between high energy dense battery and ultra high power dense conventional capacitor. The Ragone plot in Fig. 1.4 shows how supercapacitors compare to other energy storage technologies in terms of energy density and power density [3]. It clearly evidences that supercapacitors has high prospect of reaching at battery like energy density with its ultrahigh power density.

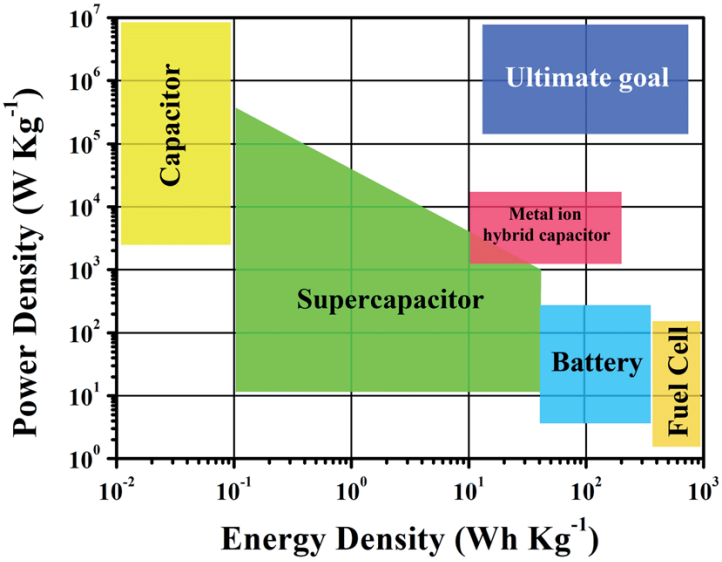

Fig. 1.4: Ragone plot of different energy storage systems.

The supercapacitors are positioned midway between the conventional capacitors and storage batteries in the Ragone plot. The capacitors can be charged instantaneously while batteries cannot be charged at this rate. When it comes to energy

storage, capacitors lag behind batteries, having very little stored energy. It is in this context we find supercapacitors, which can be charged at a faster rate than batteries and store a large amount of energy compared to conventional capacitor

1.3 Types of Supercapacitors

The super capacitor is classified into three types based on their electrochemical performance and the type of materials used for its fabrication.

1. Electrical double layer capacitors.
2. Pseudo capacitors.
3. Hybrid capacitors

The classification of super capacitors based on electrode materials are shown in Fig. 1.5.

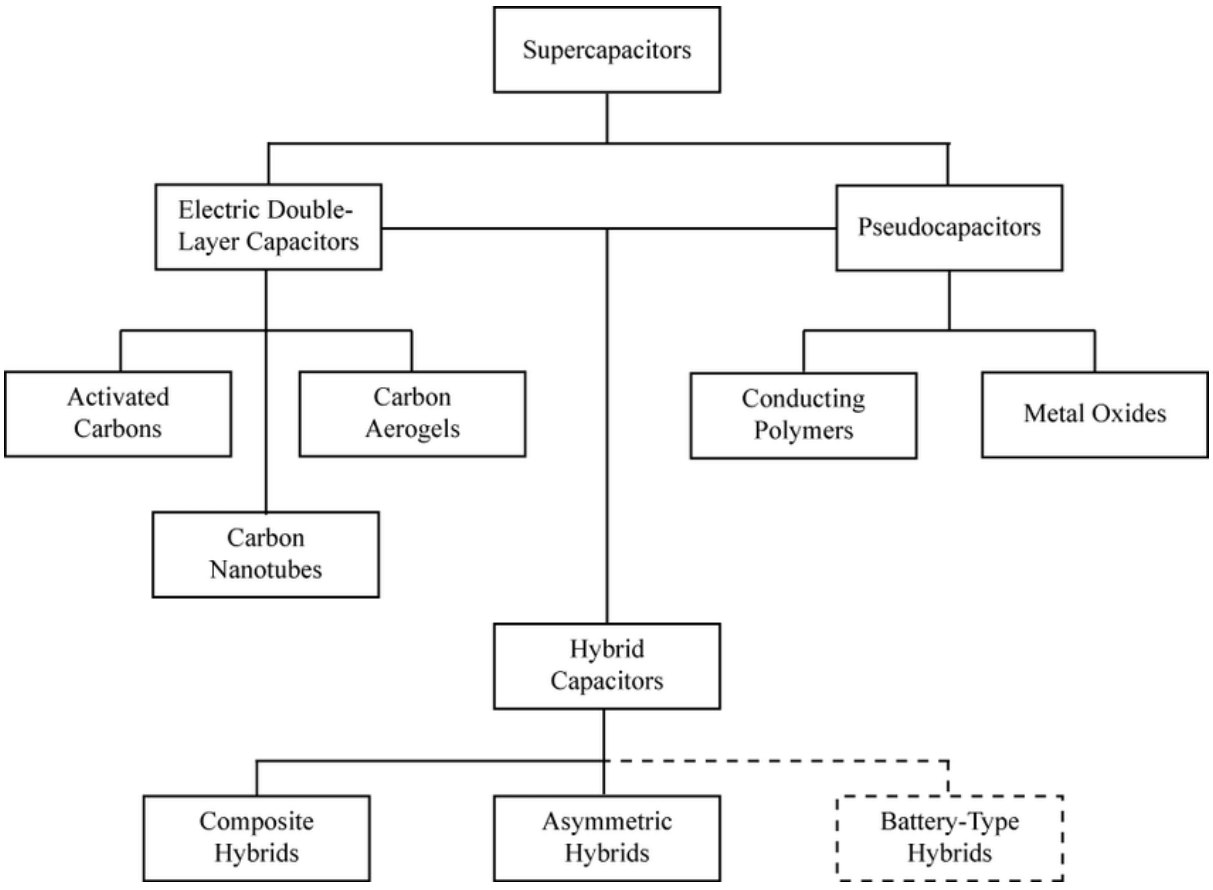

Fig. 1.5: Taxonomy of super capacitor

1.3.1 Electrochemical double-layer capacitor

The charge storage mechanism in Electrochemical double-layer capacitor (EDLC) is based on the nano scale charge separation at the electrochemical interface between the electrolyte and electrode. An EDLC is an energy storage system based on electrostatic effects that occur between two carbon electrodes with high specific surface areas per volume. The electrodes are immersed in an electrolyte. A semi-permeable membrane serves as a separator between both electrodes so as to prevent electrical contact. A schematic diagram of an EDLC is shown in Fig. 1.6. However, the separator still permits ions from the electrolyte to pass through. When the electrodes are charged, solvated ions with opposite charges are attracted towards electrode and are accumulated at the interface between electrode and electrolytic solution to form a double layer. This double layer increases with increasing specific surface area and decreasing with distance between two electrodes.

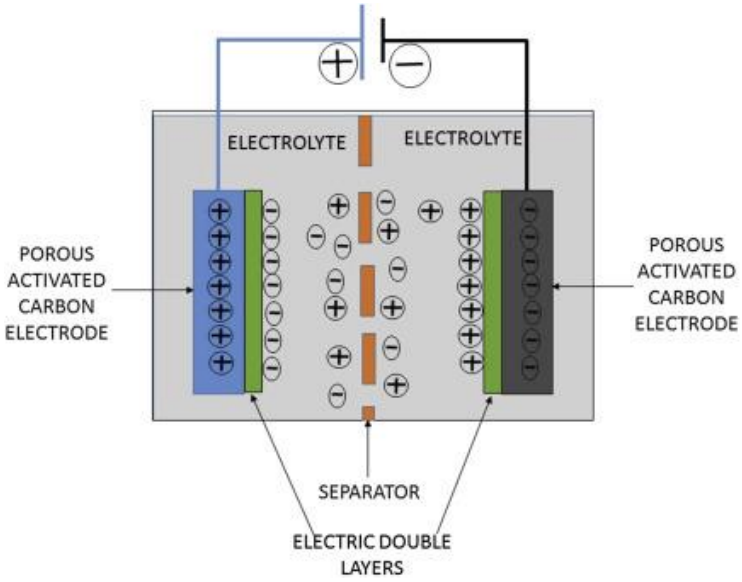

Fig. 1.6: Schematic diagram of an EDLC

EDLC's charge storage method enables for rapid energy uptake and distribution, resulting in improved power performance. It also eliminates swelling, which is common in battery electrodes, due to the lack of chemical reaction.

1.3.2. Pseudo capacitor

Unlike EDLCs, which store charge electrostatically, pseudo capacitors store charge through a faradaic process where charges transferred across the electrodes. This is achieved through electrosorption, reduction-oxidation, and intercalation processes. When a voltage is applied to

pseudo capacitor, redox reaction occurs at electrodes where charges pass occur double layer and faradaic current passes through cell. When compared to EDLC, it enables for higher specific capacitance and energy density, due to the reversible faradaic process. Transition metal oxide, conducting polymer exhibits pseudo capacitive behaviour. Even though pseudo capacitor materials have high energy density, it has poor stability and lower power density because reversible faradaic process generates swelling of electrode.

1.3.3 Hybrid Capacitor

Hybrid supercapacitors couples the advantages of both EDLCs and pseudo capacitors in a same cell. They use the combination of both faradaic and non-faradaic processes in charge storage. Hybrid capacitors have achieved energy and power densities greater than EDLCs without the sacrifices in cycling stability and affordability that have limited the success of pseudocapacitor. The carbon-based nanostructured materials as well as pseudocapacitive materials like metal oxides and conducting polymers can make hybrid energy storage system which further increases the capacitance of the composite electrode.

1.4. COMPONENTS OF SUPERCAPACITORS

1.4.1. ELECTRODE MATERIALS

Selection of electrode materials is more significant as it influences cycle life, long term stability, large surface area and resistance to electrochemical oxidation/reduction. Double layer charge storage is a surface process and the surface characteristics of the electrode greatly influences the capacitance of the cell. The electrode materials used in super capacitors are of three main categories: carbon based electrode material, metal oxide electrode material and conducting polymer electrode material.

1.4.1.1. Carbon based electrode materials

Carbon based electrode materials are considered to be potential electrode materials for EDLCs. Carbon is well known for its high surface area and hence is a suitable material for super capacitor. The main advantages of carbon based material include high conductivity, low cost, non-toxicity, wide operating range, functionality of the surface and electrochemical stability. Carbon materials with a large surface area such as activated carbon, carbon aerogels, carbon nanotubes (CNT) and carbon nano fibres can be used to make EDLCs.

Unfortunately, the high resistivity caused due to contact resistance between carbon particles leads to high internal series resistance which results in decreased electrochemical performance.

1.4.1.2. Metal oxide electrode materials

The metal oxides provide high energy density and stability for super capacitors on comparing with carbon based material. The concept and use of metal oxide as an electrode material in electrochemical capacitors was introduced by Trassatti and Buzzanca based on Ruthenium oxide (RuO_2). The metal oxide electrode's cyclic voltammogram has almost rectangular shape and exhibits good capacitor behaviour. However metal oxides are toxic and the cost of it is also very high. These electrode materials are only suitable for aqueous electrolyte and has limited operating window which forces the researchers to focus their studies on finding the environmental friendly metal oxides for supercapacitors.

1.4.1.3. Conducting polymer electrode materials

The use of conducting polymers as electrode materials in super capacitors has added advantage due to the factors such as cost, high conductivity, high potential window, adjustable redox motion via chemical variation and good storage capability. Conducting polymer based electrode materials offer pseudo capacitance behaviour through redox processes. This redox reaction in the conducting polymers affects the full mass of the material, not just the surface. This is a highly reversible reaction. But the swelling and shrinking of conducting polymers during ion intercalation/de intercalation process is a significant problem. This swelling and shrinking nature of conducting polymers leads to mechanical degradation of the electrode and reduces the cycling performance of the electrode materials.

1.4.2. ELECTROLYTES

The electrolyte is one of the most important components used in super capacitor. It serves as the transport medium from positive to negative electrode. The storage capacity of the super capacitor depends on the accessibility of ions provided by the electrolyte. Wide voltage window, high electrochemical stability, high ionic concentration, low solvated ionic radius, low .high purity and low cost are all requirements of an electrolyte for super capacitors. The

electrolytes can be classified into three categories: aqueous electrolyte, organic electrolyte and ionic liquids.

1.4.2.1. Aqueous electrolytes

Aqueous electrolytes such as H_2SO_4, KOH, NH_4Cl and so on provide higher ionic concentration and low electrochemical series resistance. These are used to obtain high specific capacitance and specific power densities in super capacitors. These can be prepared and utilized without strictly controlling the preparation procedure and conditions. However, due to the thermodynamic limit of the aqueous media the potential range over which they can operate is low. This is a significant disadvantage of aqueous electrolytes, as it limits the energy and power density of the super capacitors. The aqueous electrolytes are reported for high capacitance than organic electrolytes, due to higher concentration and small ionic radius.

1.4.2.2. Organic electrolytes

Organic electrolytes are commonly used in commercial devices, due to wide range of potential window and their higher dissociation voltage and it is a bigger advantage over aqueous electrolyte. The most commonly used organic electrolytes are acetonitrile (AN) and propylene carbonate (PC), because their electrical resistivity is at least an order of magnitude higher than that of aqueous electrolytes, resulting in capacitors with a high internal resistance. The power density of capacitor is limited by the high resistance, while the working voltage of capacitor is limited by its high water content. An organic electrolyte requires difficult purification and assembling processes in a strictly controlled environment to remove residual impurities that can lead to large performance degradation and serious self- discharge issues.

1.4.2.3. Ionic liquid electrolytes

Ionic liquid electrolytes are composed of bulky organic cations and different anions. They are solvent free electrolytes and low temperature molten salts. It has the properties such as high electrochemical stability, wide operating range, non-flammability, tunable physical and chemical properties, excellent thermal life. But its lower conductivity and expensive nature limits the applications. The physical and chemical properties of these ionic liquids depend on the type of anion and cation.

Aqueous electrolytes appear to be a superior choice among these electrolytes since they have a higher conductance, resulting in lower series resistance. Their purification

and drying processes during production are quite simple. Aqueous electrolytes are also typically less expensive than organic electrolytes.

1.4.3. SEPARATORS

The separator prevents the occurrence of electrical contact between the two electrodes, but it is ion permeable, allowing ionic charge transfer to occur. Organic electrolytes require polymer or paper separators, while aqueous electrolytes require ceramic or glass fibre separators. The separator should have a high electrical resistance, a high ionic conductance and a low thickness for best EDLC performance. The type of separator depends upon the type of electrolyte used.

1.5. APPLICATIONS OF SUPER CAPACITORS

The advantage of super capacitor is ease of disposal process because they do not contain hazardous or toxic chemicals. These supercapacitors do not need to be serviced during their lifetime and can survive a lot of charge-discharge cycles.

Supercapacitors can function at a variety of temperatures. They perform substantially better than batteries, especially at low temperatures. Owing to these advantages, supercapacitors become a good choice for applications such as electric hybrid vehicles, digital communication devices, digital cameras, mobile phones, electrical tools and uninterruptable power supplies. Significant advances have been made in improving the energy density and power density, and new applications for electrochemical supercapacitors are being developed at an increasing rate. Some of the supercapacitor applications are given below:

1.5.1. Memory Backup

Supercapacitors have long been used in electrical equipment and systems as short-term backup devices. Many appliances now have digital components with memory, and even a momentary interruption in the power supply would result in the loss of stored data. In such cases, a supercapacitor can act as the power supply for a short period, allowing data to be retained. An alternative to the supercapacitor in this application is the battery. But batteries need to be replaced regularly since batteries do not generally have a long product lifetime. Supercapacitor is a good choice for backup power supply due to their long lifetime.

1.5.2. Electric Vehicles

The possibility of using supercapacitors in electric vehicles has drawn much attention to the technology, which appeals to the energy conscious due to its energy efficiency and the ability to recover energy lost during braking. Many of the current power sources being evaluated for use in electric vehicles (EVs) do not meet the power requirements of vehicle acceleration. A combination of fuel cell and supercapacitor technology can thus provide both the power and energy requirements of an electric vehicle. Peak load requirements that result from accelerating or climbing up hills can be met by the high power device such as a supercapacitor bank. As the EDLC bank can be recharged, it can store some of the energy of an already moving vehicle and therefore increase the fuel efficiency of the electric vehicle.

1.5.3. Electrochemical Actuators

Electrochemical actuators can perform thrust vector control for spacecraft launches or can operate as flood-control actuators on submarines. The majority of actuation system require pulsed currents with high peak power but fairly moderate average power requirements. While a single supercapacitor bank is unlikely to store enough energy, a battery paired with a supercapacitor can be built to meet both average and peak load needs. Attempting to achieve both needs with a single battery results in an oversized configuration, which is undesirable in space applications where weight is limited. By designing a hybrid power source consisting of a battery and an EDLC bank can save 60 percent on weight as compared to using a battery.

1.5.4. Battery Improvement

Batteries are being used in many portable electronic devices such as laptop and mobile phones. Many of these devices use high power, pulsed currents, and current profiles that consist of short, high current bursts result in a reduction of battery performance. Therefore, using supercapacitor with battery is an optimal solution. By providing peak power requirements and allowing the battery to deliver the average load, a supercapacitor can relieve the battery of the most severe load demands. The lifetime of battery was increased due to the reduction in pulsed current drawn from the battery.

1.6 SYNTHESIS METHODS

Wide range of methods is available for the synthesis of nanomaterial. There are two general approaches for the synthesis of nanomaterial and the fabrication of nanostructure. They are top-down approach and bottom-up approach.

1.6.1 Top-down approach

A schematic diagram of top-down approach is shown in Fig. 1.7. The starting material in this approach is a macroscopic material from which nanomaterials can be synthesized by controlling some external parameters. Usually this method is not suitable for preparing uniformly shaped materials. This method has some drawbacks like contamination, but they can be fixed by employing inert atmospheres and/or high vacuum techniques etc. The biggest problem with top-down approach is the damages in structure and texture of material. Traditional top-down methods like etching or lithography could seriously harm the structure of material. During the process, new crystallographic defects could be introduced. Observations show that the nanomaterials like nanowires, nanotubes and nanosheets produced by lithography process contains a lot of contaminants and cause damage to the surface. The surface or structural changes in nanostructure could significantly alter the properties of nanomaterials. Therefore, adopting such approaches to fabricate devices may create another challenge. The ball milling method, solid state method, lithography method, physical vapour deposition etc. are examples of top-down approach.

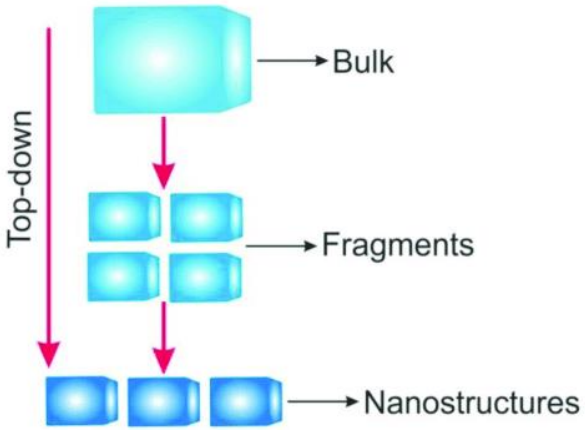

Fig. 1.7: Schematic diagram of top-down approach

1.6.2 Bottom-up approach

A schematic diagram of bottom-up approach is shown in Fig. 1.8. Bottom-up approach is a process that builds towards larger and more complex systems by starting at the molecular level and maintaining precise control of molecular structure. This method is more often used for the preparation of most of the nanomaterials with ability to generate a uniform size, shape and distribution [4]. The finest illustration is the formation of quantum dots through epitaxial growth from colloidal solution. Here, the small nuclei initiate the reaction and after that growth of nanoparticles occurs to the required size. The most popular bottom-up synthesis includes hydrothermal, sol-gel, chemical co-precipitation etc. and are discussed below.

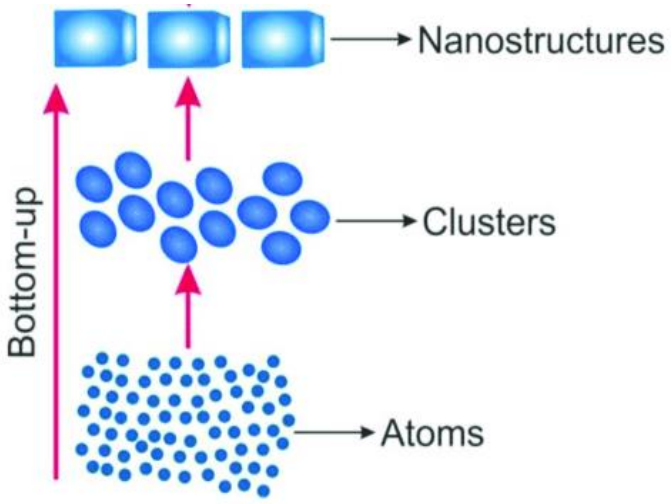

Fig. 1.8: Schematic diagram of bottom-up approach

1.6.2.1. Hydrothermal Method

Any heterogeneous system in the aqueous phase under high pressure and temperature conditions is often referred to as hydrothermal. In this procedure, chemical components that are typically insoluble under normal conditions must be dissolved and then recrystallized. However, there is no defined minimum limit of pressure and temperature. But, the majority of researchers often prefer hydrothermal synthesis at temperatures of at least 100º C and at pressures of at least 1atmosphere. The hydrothermal method is used for the synthesis of highly crystalline materials. This technique typically allows for the low temperature synthesis of materials, which would otherwise need high temperatures. To synthesize the required product using this approach, the solvent selection becomes extremely important. At or above 100ºC and with changes in pressure above 1 atmosphere, particularly at critical point,

different solvents exhibit varying characteristics. To understand the mechanism of hydrothermal reactions one should know all the properties of various solvents under different hydrothermal conditions.

1.6.2.2 Co-precipitation Method

Co-precipitation is very simple and convenient method for the synthesis of nanomaterials. This process involves co-precipitating the necessary metal cations from commonly used media such as sulphates, nitrates, carbonates and chlorides. Precursor precipitation is accomplished using chemicals like ammonia, sodium hydroxide or oxalate. In this procedure solubility is a crucial factor in precipitate formation. The separation of insoluble residue from mother liquor due to some change is called as precipitation. If any compound's concentration increases in its mother liquor the precipitation occurs as a result. This reaction occurs when the solution becomes supersaturated with respect to that compound. A supersaturated solution is one that contains more solute than allowed at equilibrium condition. Supersaturated solutions are unstable and any further increase in the concentration of solute leads to precipitation of an insoluble solid. We need to take into account the following facts in order to understand the mechanism of precipitation.

- A solution is referred to as an unsaturated solution when the concentration of a compound in the solvent is lower than its solubility product. This allows for the addition of more solute to be easily dissolved in the solution.
- A solution is referred to as a saturated solution when the concentration of compound in solution is equal to the solubility product. No additional solute gets dissolved in solution at this point.
- A supersaturated solution is formed when the concentration of compound exceeds its solubility product. It is a transient state (unstable condition), and precipitation could result with even a tiny compound addition.

1.6.2.3 Sol- gel method

In this chemical procedure, the 'sol' (solution) gradually evolves towards the formation of a gel-like diphasic system containing both liquid phase and a solid phase whose morphologies range from discrete particles to continuous polymer networks. Metal oxides or metal chlorides are used as metal precursor in this method [5]. These precursors go through hydrolysis processes and they become gel during the poly condensation process. Metal oxides

are synthesized using this technique. This procedure results in the formation of colloidal solution (sol), which serves as the basis for the gel network (gel) with discrete particles or network polymers.

1.6.2.4 Combustion Method

Combustion is a complex sequence of chemical reactions between a fuel and an oxidant accompanied by the production of heat or both heat and light in the form of either a glow or flames. The combustion uses rapid thermal degradation of precursor chemical reaction with oxygen has been effectively used for the synthesis of a variety of metal oxides in nanoscale. Based on the fuels and their combinations with the metal ions sources (commonly metal nitrates, acetates, hydroxides), combustion process has been classified into the following. Combustion of Fuel: Oxidant Fuel-oxidant combustion technique involves an exothermic decomposition of a fuel – oxidant precursors such as urea- nitrate, glycinenitrate, DHF-nitrate, etc, relatively at lower temperatures. Also, it explores highly fast and self-sustaining exothermic reaction between the metal salts and organic fuels. The heat required for the phase formation is supplied by the reaction itself and not by an external source. During this ignition process, large volume of gases will evolve which prevents the agglomeration and lead to the formation of fine powdered nanostructures. The release of heat during the combustion reaction depends on the fuel–oxidant stoichiometry in the precursor composition. The fuel–oxidant stoichiometry is used to calculate the required fuel, based on the thermodynamical concepts used in the field of propellants and explosives, for the required nature of the combustion process.

1.7 Literature Review

P. Anjali et al. investigated the performance of thin film-porous nanostructured Ce doped NiO electrodes for high performance rechargeable energy storage devices. Ce doped NiO nanoparticles were synthesized using molten salt technique and exhibited particle size of ~65nm. Substitutional doping of the NiO nanoparticles showed advantages, especially from the point of internal resistance, and improved capacitive behaviours. Doping with Ce had improved the conductivity which was reflected in the electrochemical performance and cycling stability. Based on the working model of a button cell, it has been shown that these Ce doped NiO electrodes can attain energy density and power density values of 92Wh/kg and 10kW/kg, respectively, which was found to be ~2 times higher than pristine NiO nanowires. The reduced internal resistance and the high surface area of this porous electrode system

enhance the mass specific capacitance to values as high as 1500 F/g and 1077 F/g measured from cyclic voltammetry and charge-discharge curves respectively, which was found to be ~5 times higher than the pristine NiO nanoparticles. These results are suggesting its high promising prospective for energy storage applications [6].

S. R. Gawali et al. successfully fabricated asymmetric supercapacitor using Ce doped NiO as positive electrode and reduced graphene oxide (rGO) as negative electrode in aqueous KOH electrolyte. Ce doped NiO nanoparticles were synthesized using sol-gel method. To investigate the effect of Ce doping in nickel oxide, different molar percentages of Ce with respect to nickel were incorporated. Among the different compositions, 1% Ce doped NiO exhibited high specific capacitance and excellent electrochemical activities. Thus they fabricated an asymmetric supercapacitor with 1% Ce doped NiO as positive electrode and rGO as negative electrode, which can work at an operating voltage of 1.4 V. The device achieved specific capacitance of 110F/g at a scan rate of 5mV/s with a maximum energy density of 26.27 Wh/kg. This asymmetric device exhibited excellent stability of 91.6% over 1000 cycles. This work explained the effect of Ce doping in improving the electrochemical properties of NiO [7].

M. Isacfranklin et al. synthesized pure and cerium doped nickel oxide by hydrothermal method. They studied the role of cerium dopant on nickel oxide nanostructures to tune the physico-chemical properties of the materials for energy storage applications. Structural, optical and morphological properties were studied by employing XRD, Raman, PL and SEM analysis. The information about functional group and chemical structure of the prepared sample was analysed through FTIR. Electrochemical studies exhibited good specific capacitance value of 395F/g at a scan rate of 10 mV/s for 6% cerium doped nickel oxide electrodes. This work suggested that doping of rare earth Ce metal into NiO is more suitable for supercapacitor applications [8].

P. E. Saranya et al. synthesized mesoporous ultrathin NiO and Ce doped NiO nanoflakes with 3D nanostructure of different concentrations of Ce (0.5%, 1%, 1.5% and 2%). Powder X-ray diffraction analysis was used to confirm that Ce was doped into the cubic NiO system without the formation of any secondary peaks of Ce or impurities. Average crystalline size of pristine and Ce doped NiO nanoflakes was obtained from XRD in the range of 7 to 14 nm. The FE-SEM analysis was used to explore the transformation in morphology from pristine NiO nanosheets to 3D flower-like nanostructure of Ce doped NiO nanoflakes. BET analysis

revealed that the surface area of NiO nanoflakes increased with Ce dopant concentration. 1% Ce doped NiO electrode exhibited the maximum surface area of 226.6 m^2/g which is significant for fast redox activity during charge-discharge analysis. 1%Ce doped NiO electrode offered a high specific capacitance of 2444 F/g at a scan rate of 5 mV/s, which is ~3 times higher than that of pure NiO. Electrochemical analysis results revealed the enhancement in specific capacitance of Ce doped samples over pristine NiO. The charge-discharge analysis resulted in maximum specific capacitance of 1725 F/g at 1 A/g current density for 1% Ce doped NiO nanoflakes. Electrochemical impedance spectra showed a very low resistance of 1.5Ω for 1% Ce doped NiO. 1% Ce doped NiO electrode exhibited maximum energy density of 196.04 Wh/kg and power density of 0.3112 kW/kg respectively [9].

S. D. Dhas et al. synthesized nickel oxide powder using hydrothermal method, for supercapacitor application as an efficient electrode material. The XRD study revealed that NiO powder exhibits monoclinic structure. FTIR confirmed the presence of free Ni-O bond in NiO nanoparticles. EDAX was used to confirm the existence of constituent elements such as Ni and O in synthesized NiO nanostructures. The SEM analysis showed non-uniform aggregated nanoparticles. The surface area and pore radius of NiO powder was found using BET analysis. The surface wettability measurement showed NiO surface has hydrophilic nature. NiO electrode exhibited high specific capacitances 132 F/g in KOH and 79 F/g in Na_2SO_4 electrolytes at a scan rate of 5mV/s with good cycling stability (~75% retention after 500 cycles) in a KOH electrolyte [10].

Ce doped NiO is an efficient candidate not only for supercapacitor applications but also for various applications like gas sensing and magneto-optical device fabrication. Reports suggest that doping with cerium has enhanced various properties of NiO. Effect of Ce doping on the structural, optical, magnetic, antibacterial and gas sensing properties are analysed by various authors and is discussed below.

M. Abdur Rahman et al. synthesized NiO and Ce doped NiO nanoparticles through chemical method. They studied the structural, optical, magnetic and antibacterial properties of synthesized samples. The XRD pattern revealed that the synthesized NiO and Ce doped NiO nanoparticles exhibited cubic structure. The oxidation states of Ni, Ce and O were confirmed by XPS spectra. The FE-SEM and TEM images showed the flowers with spherical nanostructures in undoped and doped NiO nanoparticles. The chemical compositions were

identified by EDAX spectra. The optical studies were carried out using UV-Visible spectra and PL studies. The results showed that the magnetization values were enhanced in Ce doped NiO nanoparticles as compared to NiO nanoparticles. This work suggests that synthesized NiO and Ce doped NiO nanoparticles can be used for the treatment of various human diseases such as pneumonia, bloodstream infection, kidney failure, wound infection and urinary tract infections[11].

Swati R. Gawali et al investigated the effect of Ce doping in enhancing the gas sensing properties. They synthesized pristine NiO and Ce doped NiO nanoparticles by sol-gel method. To understand the effect of Ce doping in NiO, various molar percentages of Ce with respect to nickel were incorporated. The structure, phase, morphology and band gap energy of synthesized nanoparticles were studied using XRD, SEM, EDAX and UV-Visible spectroscopy. Thin film gas sensors of all the samples were prepared and tested for different gases such as LPG, NH_3, CH_3COH_3 and NO_2 gas. A systematic and comparative study revealed an enhanced gas sensing performance of Ce doped NiO sensors towards NO_2 gas. It was found that 0.5% Ce doped NiO sensor shows maximum sensitivity of about 29% at moderate optimum temperature of 423K and an optimum NO_2 gas concentration of 40 ppm. This work concluded that Ce doped NiO nanoparticle gas sensors can be used as efficient and selective NO_2 gas sensors [12].

M. Naseem Siddique et al. successfully synthesized pure and Ce doped NiO nanoparticles by sol-gel method. They studied the influence of Ce^{3+} ion on the optical and magnetic properties of pure and Ce doped NiO nanoparticles. XRD analysis confirmed the single crystalline phase of the prepared samples without any impurity phase and the average crystallite size calculated from the Scherrer method follows the same trend as obtained from the Williamson-Hall method. PL spectra exhibited green emission related to oxygen vacancies and blue emission due to the Ce^{3+} ion transitions. The occurrence of mixed oxidation states of Ce ion (Ce^{3+} and Ce^{4+}) was confirmed from the XPS spectrum. The presence of Ni vacancy is found to be responsible for the observed weak ferromagnetism in pure and doped NiO samples. It was also observed that doping of Ce ions at the Ni site reduces the oxygen vacancy defect concentrations considerably. These reduced oxygen vacancies are strongly confirmed by the decreased value of luminescence intensity, remnant magnetization as well as total magnetization with increasing Ce concentration. It is suggested that improved luminescence with Ce^{3+} ion transitions and ferromagnetism with the intrinsic

defects may have many applications such as novel magneto-optical devices and spintronics [13].

Muthukumaran P. et al. designed Ce doped NiO nanomaterial as an efficient platform for the detection of riboflavin (RF). They synthesized Ce doped NiO nanostructures via hydrothermal method. Ce doped NiO nanomaterial exhibited an excellent performance together with high sensitivity, selectivity and stability. They also evaluated the antimicrobial activity of Ce doped NiO nanostructures. Results indicated that Ce doped NiO nanostructures exhibited excellent antibacterial activity against *K. pneumonia, S. typhi, P. aeruginosa, B. cereus, B.subtilis* and *S. aureus.* From the results, it was evident that Ce doped NiO nanomaterial is a useful platform for electrocatalytic and biomedical applications [14].

Ling Zhu et al. synthesized pure and novel Ce doped NiO hierarchical micro flowers using a facile one-step hydrothermal method. A comparative ethanol sensing investigation between the pure and cerium doped NiO micro flowers was subsequently performed. In comparison to the pure sample, the Ce doped NiO micro flowers exhibited superior ethanol sensing properties. The higher sensor response is primarily responsible for the unique hierarchical nanostructure and the change in effective hole concentration due to the incorporation of Ce into NiO [15].

Norliza Dzakaria et al. investigated the reduction behaviour of pure NiO and Ce doped NiO catalysts by using temperature programmed reduction (TPR) technique with exposure of 40% carbon monoxide (CO) in nitrogen atmosphere as a reductant agent. The cerium doped NiO catalysts were prepared using the conventional impregnation method. The particles were characterized by XRD, BET, FE-SEM and EDAX analysis. XRD diffractogram of the catalysts showed a complete reduction of NiO to Ni. The interaction between cerium and nickel ions for Ce doped NiO series leads to a slight decrease in the reduction temperature. Fine particles of Ce deposited on the NiO surfaces were observed through FE-SEM images indicating some morphology modification occurred on NiO. The results showed that the addition of Ce to NiO has a remarkable influence in reducing the temperature of the reduction process. The 5% Ce doped NiO was found sufficient to enhance the reductibility of NiO at a lower temperature [16].

1.8 Objectives

- To synthesize NiO and 1% Ce doped NiO nanoparticles using modified auto combustion method.
- To study the structural and morphological properties using XRD, FE-SEM and EDAX.
- To study the optical properties of the material using UV-Visible spectroscopy and to determine the bandgap.
- To analyse the characteristic vibrational modes using Raman and FTIR spectra.
- To investigate the effect of doping on the supercapacitor performance of the material.

CHAPTER 2

SYNTHESIS METHOD AND CHARACTERIZATION TECHNIQUES

2.1 Synthesis

Nanostructures of pristine and Ce-doped NiO are synthesized using a modified auto combustion method. A stoichiometric amount of nickel nitrate hexahydrate (merk, 98% purity) and citric acid (merk, 98% purity) are taken for the preparation of pristine NiO and cerium nitrate hexahydrate, citric acid, and nickel nitrate hexahydrate for $Ni_{(1-x)}Ce_xO$ (x = 0.00, 0.01) nanostructures. The mixture is dissolved in deionized water wherein citric acid is used as a complexing agent. 30 ml of nitric acid is added to the above solution. A solution with no precipitation and sedimentation is obtained after 30 minutes of stirring. Ammonia is added to maintain the pH as neutral. The solution is heated on a hot plate at about 250 ºC in the combustion chamber. On the completion of dehydration, internal combustion starts, and a black coloured powder is obtained. The resultant powder is heated to about 600 ºC for 3 hrs in the high-temperature furnace to remove impurities. The sintered samples are taken for different characterizations.

2.2 Characterization Techniques

It is important to analyse the synthesised samples using different characterization techniques to ensure that the desired product has formed. These techniques are also used to investigate the structural, morphological, magnetic, and dielectric characteristics of prepared samples. The following section discusses various characterization methods that have been used to analyse prepared samples.

2.2.1 X-ray Diffraction Technique (XRD)

X-ray diffraction is a rapid analytical technique primarily used for phase identification of a crystalline material and can provide information on unit cell dimension.

Its application includes:

- Characterization of crystalline materials
- Measurement of sample impurity

- Identification of fine-grained minerals as clays and mixed layer clay that are difficult to determine optically
- Determination of unit cell dimensions
- Determine crystal structures using Rietveld refinement
- Determination of modal amounts of minerals

Max Von Laue, in 1912, discovered that the crystalline substances act as 3 dimensional diffraction gratings for x-ray wavelengths similar to the spacing of planes in a crystal lattice. X ray diffraction is now a common technique for the study of crystal structures and atomic spacing.

X-ray diffraction is based on constructive interference of monochromatic X-ray diffracted from sample. These X-rays are generated by a cathode ray tube, filtered to produce monochromatic radiation, collimated to concentrate and directed towards sample. The interaction of the incident rays with the sample produces constructive interference when condition satisfies Bragg's law as shown in the Fig. 2.1. This law relates the wavelength of electromagnetic radiation to the diffraction angle and lattice spacing in crystalline sample.

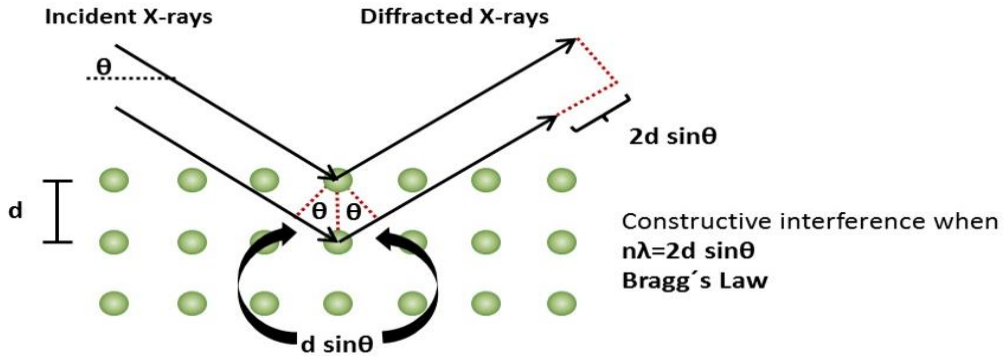

Fig. 2.1: Schematic representation of Bragg equation

Working of XRD

An X-ray diffractometer consists of three basic components: X-ray source, sample holder and X-ray detector. X-rays are generated in a cathode ray tube by heating a filament to produce electrons. Due to the applied voltage, electrons are accelerated and bombarded on the target material. If the electrons have enough energy to dislocate electron from the inner shell of target material, XRD spectra are generated. An X-ray radiation with a certain amount of

energy is released when an electron from the outer shell fills the vacancy created in the inner shell. In XRD, the targets are often Cu and Mo. These emit 8 keV and 14 keV energy which corresponds to1.54 and 0.8 angstrom wavelength respectively.

These X-rays are collimated and directed onto the sample. X-rays interacts with the electrons of the atoms. The scattered waves from different atoms can interfere with each other and give rise to the diffraction effect [17]. When the geometry of incident x-ray impinging the sample satisfies the Bragg's equation, constructive interference occurs and a peak in XRD is generated. Figure 2.2 shows the X ray diffractometer.

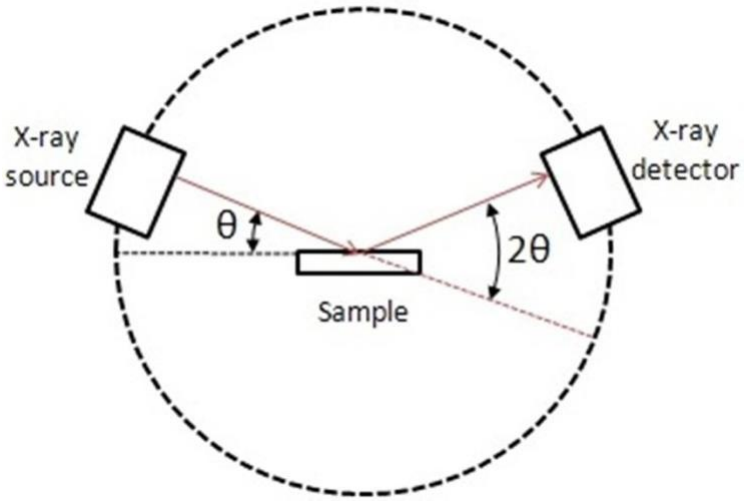

Fig. 2.2: X-ray diffractometer

From obtained diffraction pattern, the distance between crystal planes can be calculated using Bragg's law. The law states that

$$n\lambda = 2d \sin\theta$$

where, $\lambda \longrightarrow$ wavelength of the X rays

$d \longrightarrow$ spacing between layers

$n \longrightarrow$ order of diffraction

$\theta \longrightarrow$ angle of incidence

The powder method uses a large number of tiny crystals that are orientated in every direction conceivable. As a result, all sets of planes scatter X-rays. A film that is X-ray sensitive is used to detect the scattered X-rays. The substance to be analysed is retained in the sample holder as a thin film and is finely powdered. X rays are allowed to fall on the powder. A strip of photographic film prepared in the shape of a circular arc is exposed to the diffracted X-

rays. As a result, we get lighted areas in the form of arcs or lines at different distances from the incident beam. To utilise Bragg's equation for various crystal planes, these lengths can be transformed into scattering angles. The incident X-rays are measured at one fixed point though it might be scattered in different direction. Hence we need angle of incidence to be equal to that of angle of reflection. This can be achieved by moving detector twice faster than θ angle of source. A plot between angle 2 theta with intensity is thus obtained and used for analysis. The analysis of XRD data provides information of phase purity, unit cell parameter, particle size, X-ray density and distribution of cations.

The average crystallite size of the particles at highest intense peak may be determined from the Scherrer's formula

$$D = k\lambda/cos\theta$$

where, crystallite size, Bragg's angle of diffraction in degrees and shape factor (taken as 0.9) are assigned by D, θ, k and λ is the X-ray wavelength (1.54Å).

2.2.2 Field Emission Scanning Electron Microscopy (FE-SEM)

Field Emission Scanning Electron Microscopy, also known as FE-SEM, is one of the versatile techniques used to examine the morphology of microstructures and provide information on the distribution and shape of nanoparticles. The scanning electron microscopes have many advantages over light microscopes [18]. It also has higher resolution; hence closely spaced specimens can be magnified at higher magnifications.

Construction and working of FE-SEM

This instrument consists of an optical electron system for producing an electron probe, a specimen stage for placing the sample, a secondary electron detector for gathering secondary electrons, an image display unit and an operating system for performing varied operations. The optical electron system consist field emission electron gun, a condenser lens and an objective lens. Basic construction of FE-SEM is shown in Fig. 2.3.

FE-SEM employs a fine electron beam to create magnified image of the sample instead of light. A stream of monochromatic electrons is produced by the electron gun, placed at the top of the microscope. This beam travel downward through a series of magnetic lenses designed

to focus the electrons to a very fine spot. When electron beam hits the sample, electrons and X-rays are ejected from it.

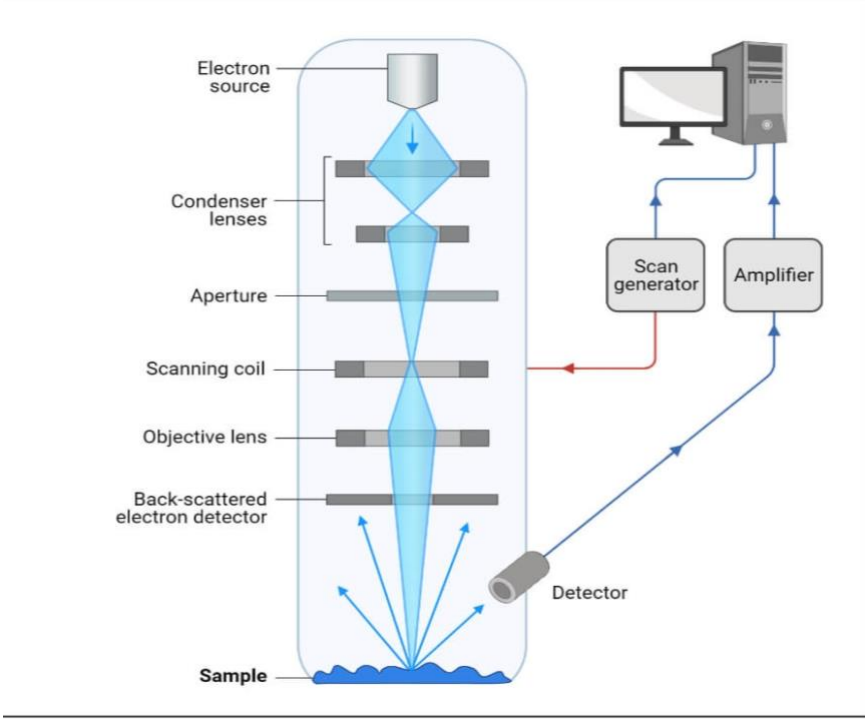

Fig. 2.3: Basic construction of FE-SEM

Fig. 2.4 shows interaction of incident beam on the matter which produces X-rays, Auger electrons, primary back scattered electrons, secondary electrons. X-rays, backscattered electrons and secondary electrons are collected by the detectors and converted into a signal which is finally sent to a screen on which final image is produced. The back scattered electrons are in charge of the atomic number contrast and give information about sample composition, whereas the secondary electrons are responsible for the topological contrast and provide information about surface morphology.

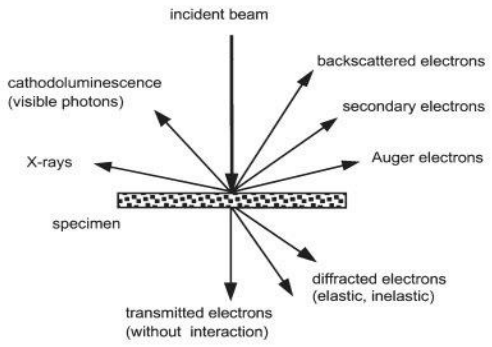

Fig. 2.4: Interaction of incident beam with sample

The sample being examined by FE-SEM must be of a conductive type and be present in sufficient quantities to mount rigidly on the sample holder called the specimen stub. By using a technique known as sputter coating, nonconductive samples are often covered in an ultrathin layer of conductive material such as gold, tungsten, indium, and graphite. The advantage of FE-SEM is that it offers a relatively wide magnification range, allowing the researcher to easily focus in on the particular region of the specimen that was initially scanned at lesser magnification. As a result, this instrument is much more than just a tool for morphology observation; it also has the ability to perform elemental analysis and state analysis.

2.2.3 Energy Dispersive Spectroscopy (EDAX/EDS)

It is an investigative method which is widely employed in elemental or chemical characterization of objects. The sample may be of any form such as solid thin films, solid powder, liquid sample, or even a pellet etc. Also known as Energy dispersive analysis of X-rays and can be abbreviated as EDAX, EDS or EDX. The interaction of an electron beam with a sample produces various forms of emissions, which are detected by Energy Dispersive X-ray spectroscopy as characteristic X-rays of various elements. The corresponding energy spectrum is used to obtain information about the chemical composition of a material. The typical set up of EDAX is similar with that of SEM set up. The sensitive X ray detector, liquid Nitrogen for cooling and software to record energy spectrum are main components of this spectrometer. In the sample chamber of the main system, the detector is located at the end of a long arm with a liquid nitrogen cooling system. Detectors are generally made of Si (Li) crystals that can work at low voltages to enhance sensitivity. Current technology known as, ‘Silicon drift detectors’, operate at higher count rates without the need for liquid nitrogen cooling. The detector is made up of a crystal that absorbs the energy of X-rays through ionization, releasing free electrons in the crystal and making it conductive, resulting in an electrical charge bias. The energy of individual X rays is consequently transformed into an electrical voltage that corresponds to the element's characteristic X-rays. As a result, EDAX is a tool for determining the chemical composition of a sample at the surface and near surface. The key hindrance is the overlap of energy peaks among various elements.

2.2.4 Raman Spectroscopy

Raman spectroscopy can be used to determine the vibrational levels of a compound. It was extensively used in chemistry to identify compounds by their fingerprint. Raman spectroscopy is the study of matter by the inelastic scattering of monochromatic light. The underlying principle behind Raman spectroscopy is illustrated by comparing it with infrared spectroscopy. The molecule makes a transition from its ground state to its vibrationally excited state by the absorption of infrared rays. This was only possible when the absorbed energy is equal to the differences in energies of ground and excited state. We get more information about the sample by illustrating the frequency of infrared photons that the molecule absorbs and elaborating these frequencies with regard to characteristic vibrational modes of a system. The IR and Raman scattering was almost the same. Raman spectroscopy differs from infrared spectroscopy in that the photons involved were shifted in frequency with an arrangement equivalent to the energy of a certain vibrational transition rather than being absorbed or emitted.

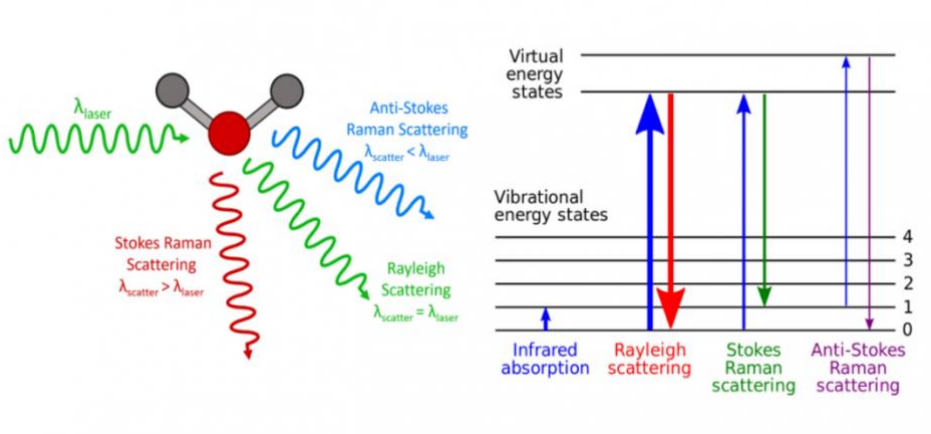

Fig. 2.5: Raman spectroscopy principle

Raman scattering involves three types of scattering: Rayleigh, Stokes, Anti-stokes scattering. Most of the molecules are initially in the ground state (labelled 0 in the figure) but because of thermal agitation some molecules will be in an excited state (labelled 1). The scattering process can be thought of as the incoming photon raising the molecule to a virtual excited state. But since the molecule cannot remain in this virtual level, it must immediately fall back down to a lower level with the emission of a photon. If the molecule falls into the same level as it started from, there is no frequency shift in the emitted photon and is called Rayleigh scattering. If the molecule falls into a different level, the energy of emitted photon must differ

from that of the incoming photon. In this case, the emitted photon has a different frequency from that of incident photon, this process is called Raman scattering. The frequency can decrease (give rise to Stokes line in the spectrum) or increase (anti-stokes), depending on whether the molecule starts in the ground state or an excited state.

A Raman spectrometer consists of an excitation source, usually a laser, sample illumination system, a double or triple monochromator and a signal processing system containing a detector, an amplifier and an output device. Raman spectroscopy has applications in many fields. Raman studies are potentially useful sources of information concerning the composition, structure and stability of coordination compounds. It is used to study the chemical bonding and for identifying molecules. It is used to characterize materials and it is very helpful for finding the crystallographic orientation. Raman spectroscopy has been applied widely for the study of biological systems.

2.2.5 Fourier Transform Infrared Spectroscopy (FTIR)

FTIR is the most effective chemical detection method used to identify unknown materials and to determine the amount of components in a mixture. By creating an infrared absorption spectrum that resembles a molecular "fingerprint," it is an effective tool for defining the different kinds of chemical bonds that exist in molecules and for identifying different configuration modes of functional groups that are present in the nanomaterial being synthesised [19]. The specific qualities of the chemical bond are represented by the wavelength of light that is absorbed. Like a fingerprint, no two unique molecular structures produce the same infrared spectrum. This makes infrared spectroscopy useful for several analysis.

Construction and working of FTIR spectroscope

An FTIR spectrometer consists of IR source, interferometer (beam splitter, fixed mirror, moving mirror), detector and a Fourier transform. The most common source for the mid-IR range, which covers wavelengths between 5000 and 4000 cm^{-1}, is a silicon carbide element heated to about 1200 K. For the near-IR range, which covers wavelengths between 10,000 and 4,000 cm^{-1}, requires a higher temperature source and a tungsten halogen lamp is typically used, and for the far-IR range, a mercury discharge lamp for wavelengths greater than 200 cm^{-1} provides a higher output than a thermal source. A schematic diagram for FTIR spectroscopy is shown in Fig. 2.6.

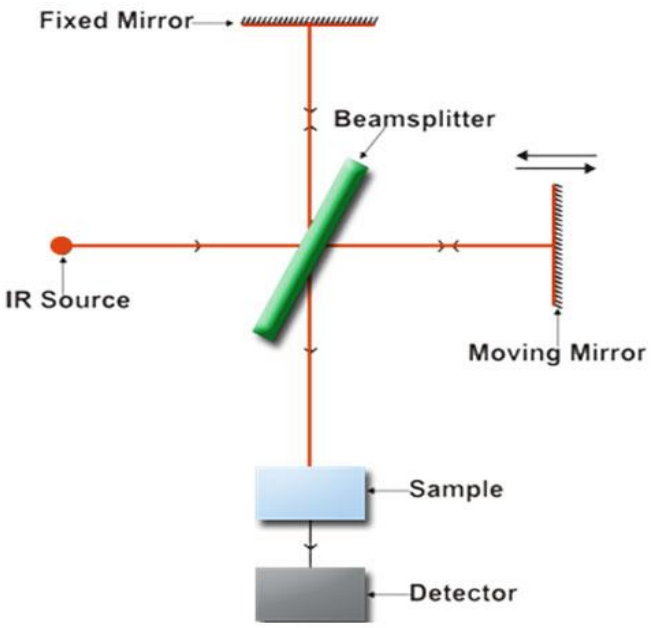

Fig. 2.6: Schematic diagram for FTIR spectroscopy

Infrared energy is emitted from the IR source and allowed to incident on the beam splitter which transmits and reflects 50% of the incident radiation. The moving mirror reflects the transmitted beam, and the fixed mirror reflects the reflected beam from the beam splitter. These reflected beams from the fixed and moving mirrors comeback and combine together at the beam splitter resulting both the constructive interference (zero path difference) with high intensity and destructive interference (optical path difference) with low intensity and the beam get transmitted out of the interferometer with low and high intensity incident on the sample. If the transmitted light's energy matches that of the sample's molecules, it is absorbed by the sample and causes the molecules to vibrate. If the energy of the transmitted light does not match, it passes through the sample and is detected by the detector to create an interferogram, which is the plot between energy and time. On applying Fourier equation, Fourier transform allows to convert intensity verses time spectrum into an intensity versus frequency spectrum through which we can make interpretation about various molecules or functional groups present in the sample.

2.2.6 Ultraviolet Visible (UV-Visible) Spectroscopy

UV-Visible Spectroscopy is an analytical technique which is used to study the interaction between electromagnetic radiation and matter. UV-Visible spectroscopy refers to absorption spectroscopy or reflectance spectroscopy in the ultraviolet-visible spectral region (190-

780nm). This means it uses light in the visible and adjacent (near UV and near infrared (NIR) ranges. This spectroscopy is routinely used in analytical chemistry for the quantitative determination of different analysis such as transition metal ions, highly conjugated organic compounds and biological macro molecules. The Beer-Lambert law states that the absorbance of a solution is directly proportional to the concentration of absorbing species in the solution and the path length. Thus, for a fixed path length, UV-Visible spectroscopy can be used to determine the concentration of absorber in a solution.

A UV-Visible spectrometer consists of a light source, a sample holder, a monochromator and a detector. The hydrogen discharge lamp is the most commonly used source of radiation in the UV region (190-400nm). A deuterium discharge lamp is used in its place when more intensity is desired. A tungsten filament lamp is used when absorption in the visible region (400-780 nm) is to be determined. A schematic diagram of a UV-Visible spectrometer is shown in the Fig. 2.7.

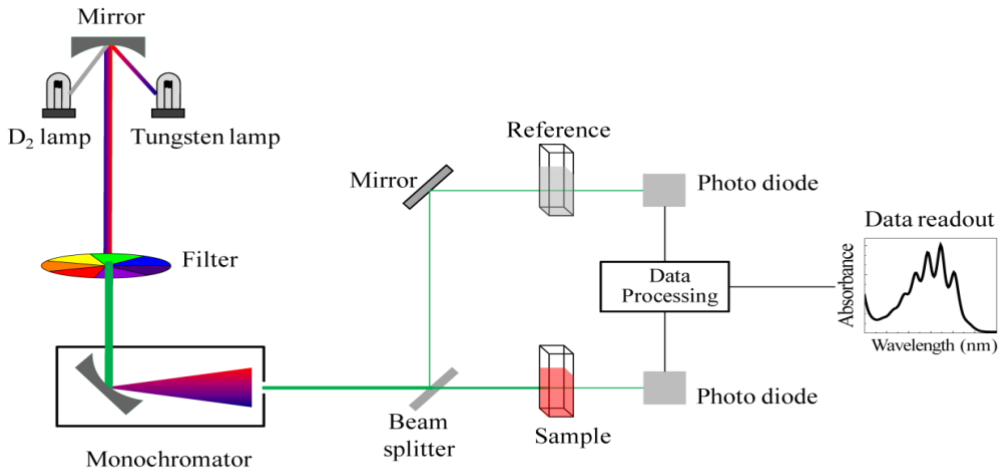

Fig. 2.7: Schematic diagram of UV-Visible spectrometer

Monochromator disperses the radiations obtained from the source into their separate wavelengths. The most widely used dispersing element is a prism or grating made up of quartz. The dispersed radiation is allowed to fall on a beam splitter where the radiation is split into two parallel beams. One beam is used as the reference and the other beam passes through the sample. The reference beam intensity is taken as 100% transmission (or 0 absorbance)

and the measurement displayed is the ratio of the two beam intensities. Some instruments have two detectors (photodiodes), and the sample and reference beam are measured at the same time. Samples for UV-Visible spectrometry are most often liquids, although the absorbance of gases and even of solids can also be measured.

2.2.6.1 Determination of band gap -Tauc plot

The Tauc method of determining the optical absorption edge of materials is a well-known technique used to characterize functional photovoltaic layers, transparent conductors, sensor coatings, and films for many other applications. This method was originally designed for determinations of absorption in amorphous thin-film materials. Since then, the tauc method has widely used on crystalline thin films as well. Because UV-Vis spectrometers are widely available, easy to use, and the absorbance equation is well understood, the Tauc method is often used instead of more accurate means. In the Tauc method, broad spectral absorption spectroscopy results are fitted using a power-law expression. The photon-energy axis intercept of this fit then reveals the bandgap of the material in question, and the fitted exponent indicates either a direct or indirect electron transition.

While investigating the optical and electronic properties of amorphous germanium, Tauc et al proposed and substantiated a method for determining the band gap using optical absorbance data plotted appropriately with respect to energy. This was further developed in Davis and Mott's more general work on amorphous semiconductors, which showed that the optical absorption strength depends on the difference between the photon energy and the band gap as $\mathbf{(\alpha h\upsilon)^{1/2} = A(h\upsilon - Eg)}$ where h is Planck's constant, n is the photon's frequency, α is the absorption coefficient, E_g is the band gap, and A is the slope of the Tauc plot in the linear region. The value of the exponent denotes the nature of the electronic transition, whether allowed or forbidden and whether direct or indirect:

For direct allowed transitions: n = $\frac{1}{2}$

For direct forbidden transition: n = $\frac{3}{2}$

For indirect allowed transitions: n = 2

For indirect forbidden transitions: n = 3

Typically, the allowed transitions dominate the basic absorption processes, giving either n = $\frac{1}{2}$ or n = 2 for direct and indirect transitions, respectively.

Thus, the basic procedure for a Tauc analysis is to acquire optical absorbance data for the sample in question that spans a range of energies from below the band gap transition to above

it. Plotting the as $(\alpha h\upsilon)^{1/n}$ versus as $(h\upsilon)$ is a matter of testing n-values (either n = $\frac{1}{2}$ or n = 2) to find which provides the best fit and thus identifies the correct transition type and where the energy-axis intercept gives the band gap value. In the indirect case, there will always be higher energy transitions that can happen by a direct process, too. In this case, it might be possible to extract both indirect and direct edges with plots using the appropriate exponents

2.3 Electrochemical Characterization

To test the capacitance of materials, two electrochemical methods, Cyclic Voltammetry (CV) as well as Galvanostatic Charge/Discharge (GCD), are used.

2.3.1 Cyclic Voltammetry

Cyclic Voltammetry or CV is a type of potentiodynamic electrochemical measurement. It is a powerful and popular electro-chemical tool to examine the reduction and oxidation processes occurring within the molecular species. It is used to investigate the mechanism, kinetics and thermodynamics of both homogeneous reactions in the solution and heterogeneous reactions occurring at the electrode surface. A typical CV records the current flowing between the working and counter electrodes for a specific potential window by varying the scan rates. Cyclic voltammetry is generally used to study the electrochemical properties of an analyte in solution [20]. The electrode potential ramps linearly versus time in cyclic voltammetry, as shown in Fig. 3.1. This ramping is known as scan rate (V/s) of the experiment.

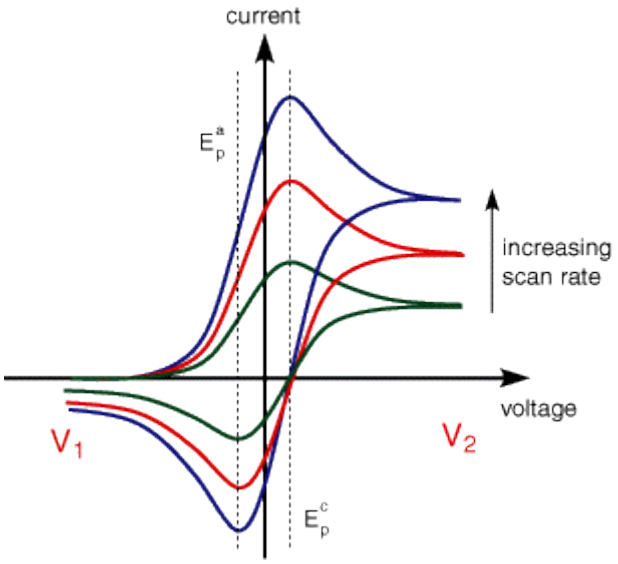

Fig. 3.1: Scan rate dependence

The potential is applied between the reference electrode and the working electrode and the current is measured between them. This data is then plotted as current (I) versus potential (E). For any analytes that can be reduced (or oxidised, depending on the initial scan direction) within the range of the potential scanned, scan generates a current peak. . The current will rise as the potential reaches the reduction potential of the analyte, but then it will falls off as the concentration of the analyte near the electrode surface depletes. If the redox couple is reversible then when the applied potential is reversed, it will reach the potential that will reoxidize the product formed in the first reduction reaction, and produce a current of reverse polarity from the forward scan. Usually, the shape of this oxidation peak will resemble that of the reduction peak. As a result, information about the redox potential and electrochemical reaction rates of the compounds is obtained. The current peak will be proportional to the square root of the scan rate, if the electronic transfer at the surface is fast and the current is limited by the diffusion of species to the electrode surface.

Cyclic voltammetry measures charge-response with regard to a changing voltage and is therefore a means to evaluate capacitance. In a CV analysis, the current response is recorded for a series of applied changing voltages at a constant sweep rate (dV/dt). An ideal capacitor with no resistance would display a rectangular shape. The specific capacitance was calculated using half the integrated area of the CV curve to obtain the charge (Q), and subsequently dividing the charge by the mass of the film (m) and the width of the potential window (ΔV)

$$C = \frac{Q}{m\Delta V}$$

Faster sweep rate corresponds to charging and discharging at higher power levels. Multiple plots obtained at increasing sweep rates are therefore displayed on the same graph to demonstrate the effect of power levels on the charging characteristics. It is clear from such plots that the capacitance decreases at higher scan rates.

2.3.2 Galvanostatic Charge Discharge (GCD)

The Galvanostatic charge discharge (GCD) technique is a method to evaluate the electrochemical capacitance of materials under controlled current conditions. In GCD, the instrument operates in the galvanostatic mode to control current and measure voltage. Usually a constant current flows between two electrodes; the potential of one electrode is

monitored as a function of time with respect to the suitable reference electrode. Applications for this method include plating or measuring battery charge/discharge curves. In order to test the performance and cycle-life electrochemical double layer capacitors and batteries, cyclic charge-discharge is the standard technique used. The capacity of each cycle is measured and the capacitance (C) is calculated by the equation

$$C = \frac{I\Delta t}{\Delta V}$$

where I is the constant applied current (A), Δt is the cycle time and ΔV is the potential difference. Generally, cycle number indicates how many times the battery can undergo the process of complete charging and discharging until it starts losing its capacity.

2.3.3 Electrochemical Impedance Spectroscopy (EIS)

Electrochemical impedance spectroscopy (EIS) is an electrochemical technique frequently used for investigating electrochemical systems and processes. It is a high precision measurement technique mostly used for characterizing the interfacial and the bulk properties. Electrochemical system comprises of interfaces and simultaneously occurring process such as the electrode-solution interface, contributions from the electrolyte and the electrochemical reactions happening on the electrode which contribute to the total impedance of the system. The concept of impedance is associated with the AC (alternating current) whereas the term resistance is a used for DC (direct currents). Hence EIS can determine both passive (resistance) and active (capacitance, inductance, diffusion) components efficiently.

.

Chapter 3

Results and Discussions

XRD

The XRD analysis reveals the structural information, phase purity and average crystallite size of the prepared nanoparticles. XRD patterns of NiO and $Ni_{0.99}Ce_{0.01}O$ is shown in Fig 3.1. The XRD profile of pure NiO have diffraction peaks at 37.00° , 42.96°, 62.70°, 75.18° and 79.24° and are indexed to the (111), (200), (220), (311) and (222) reflection planes of single phase face-centered cubic structure with a space group of Fm-3m [21].

Observed peaks are in good agreement with JCPDS card number 780643. The diffraction peaks of dopant materials are identical to the XRD pattern of pristine NiO. It indicates that Ce doping has not changed the crystal structure of nickel oxide. Moreover, absence of any peak corresponding to CeO2 phase confirms the purity of the sample even after doping [22].

Shift in the peaks towards higher theta values and the decrease in intensity values after doping indicates the presence of local distortion of NiO crystal lattice due to doping of Ce. Since, the ionic radii of Ni^{2+} and Ce^{4+} are 69 p.m. and 101 p.m. respectively, the higher ionic radius of Ce^{4+} could create a local distortion and strain in the crystal lattice of NiO. Lattice parameters are listed in Table 3.xx which shows an increment in parameters with doping which is due to the lattice expansion due to doping with Ce^{4+} having higher ionic radii. Higher ionic radii of dopant lead to the expansion in unit cell volume with increase in dopant concentration. The average crystallite size of prepared nanoparticles was obtained from the Debye-Scherrer formula,

$$D = \frac{k\,\lambda}{\beta \cos\theta}$$

Where, D stands for average crystallite size, k for shape factor (0.90), λ for wavelength of X-ray for Cu-kα radiation,(λ =1.5406 Å), β is the full width at half maximum and θ in degree for diffraction angle.

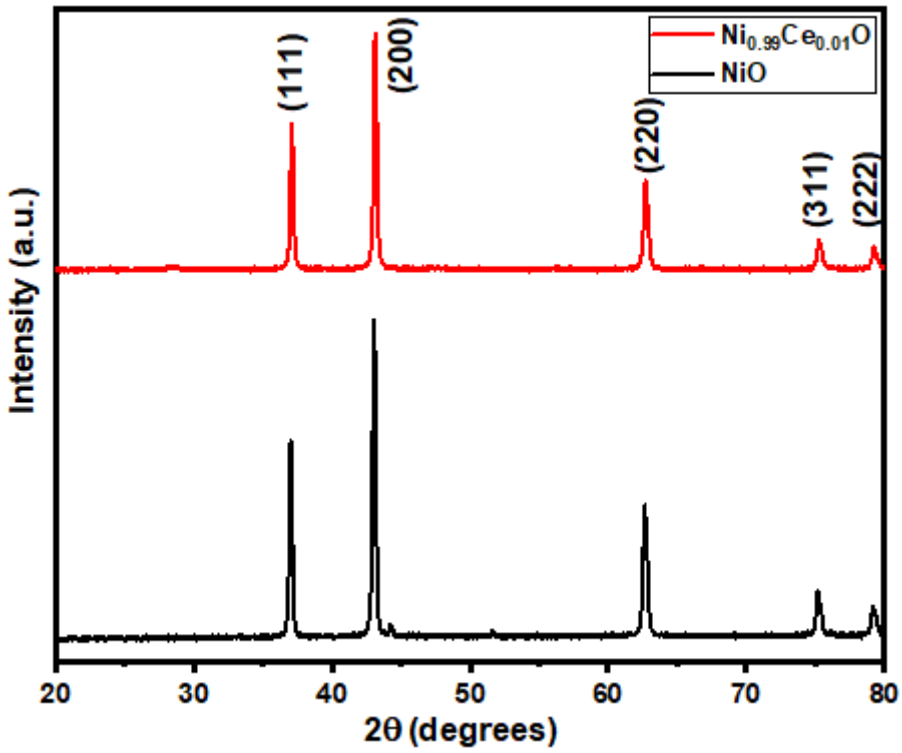

Fig 3.2: XRD patterns of NiO and $Ni_{0.99}Ce_{0.01}O$

Table 3.1: Lattice parameters and crystallite size of NiO and $Ni_{0.99}Ce_{0.01}O$

Sample	Lattice constants				Crystallite size
	a(Å)	c(Å)	c/a	V (Å^3)	(nm)
NiO	4.1736	4.1736	4.1736	72.6988	25.0530
$Ni_{0.99}Ce_{0.01}O$	4.1759	4.1759	4.1759	72.8217	24.6538

Rietveld Refinement

Fig. 3.2 shows the Rietveld refinement of NiO and $Ni_{0.99}Ce_{0.01}O$ and the refinement parameters are listed in Table. 3.2. Formation of phase pure NiO is confirmed using Rietveld refinement.

Table 3.2: Refinement parameters of NiO and $Ni_{0.99}Ce_{0.01}O$

Sample	R_p	R_{wp}	R_e	χ^2
NiO	3.31	4.30	3.52	1.50

$Ni_{0.99}Ce_{0.01}O$	4.78	6.61	3.76	3.08

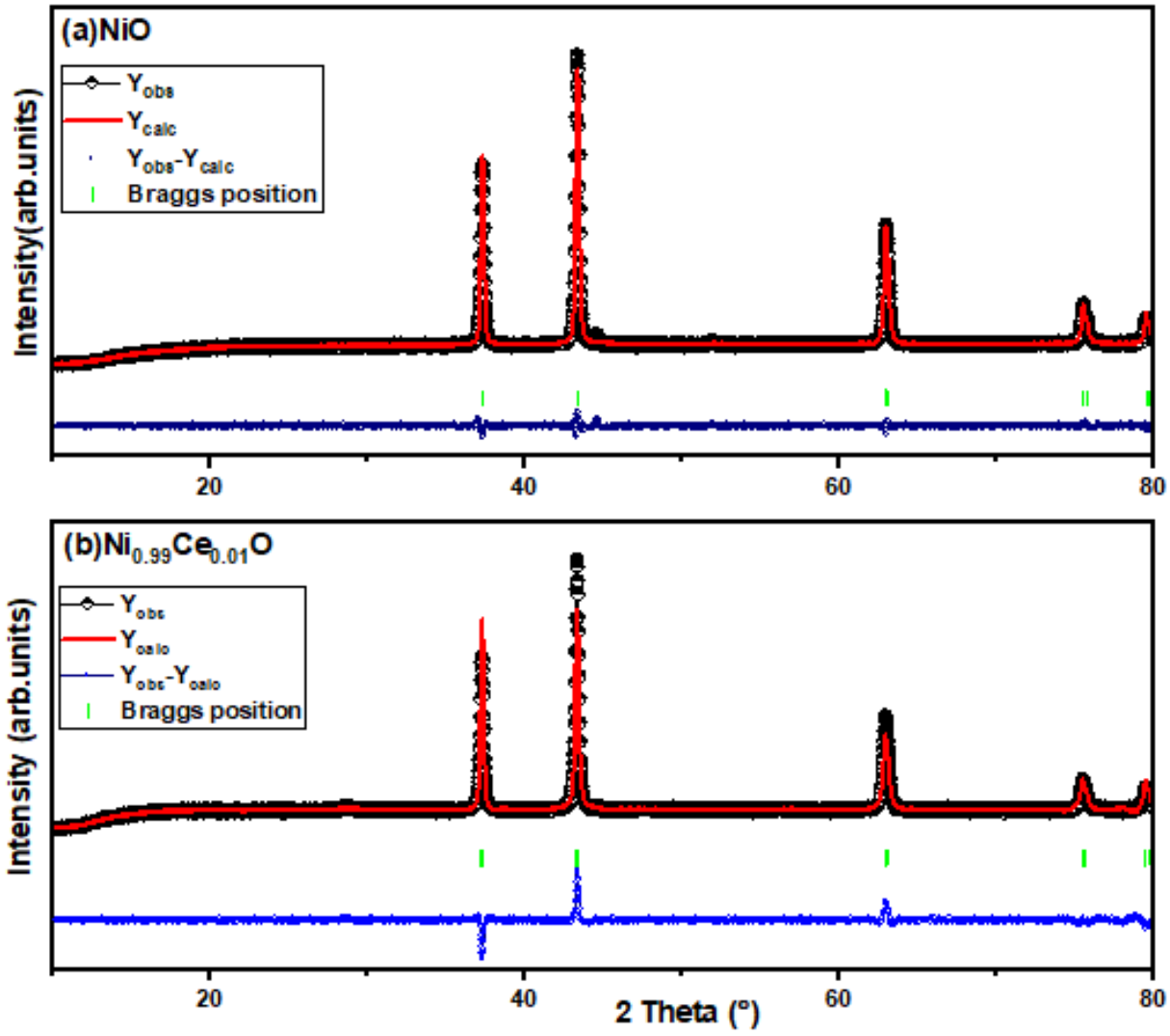

Fig. 3.3: Refinement patterns of NiO and $Ni_{0.99}Ce_{0.01}O$

FE-SEM

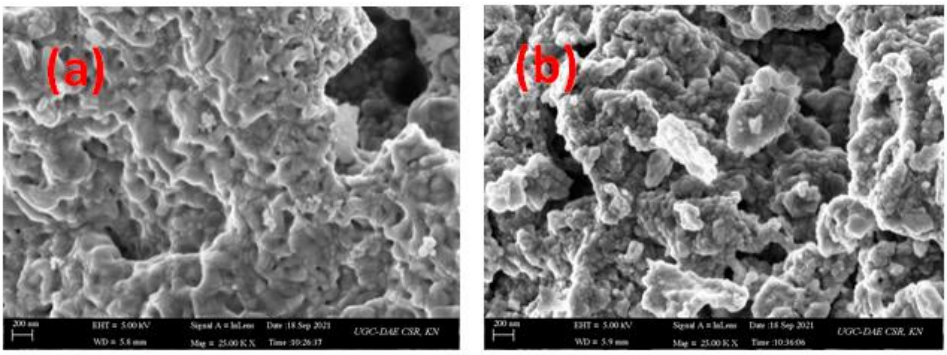

Fig. 3.4 (a) FE-SEM of NiO & (b) FE-SEM of $Ni_{0.99}Ce_{0.01}O$

Morphological evolution of NiO and $Ni_{0.99}Ce_{0.01}O$ are evaluated using FE-SEM and is given in Fig 3.3. FE-SEM image shows the formation of non-uniform agglomerated spherical particles. There exist small spaces between the nanostructures and it is found to be increased with doping. The observed morphology is having porous structure with wrinkles on the surface. Low concentration doping of Ce do not affect morphology of the sample to a great extent even though uniformity increases. [23]

EDAX

EDAX spectra given in Fig. 3.4 is used to analyse the weight percentage of the elements in the samples. Chemical composition of the nanostructures is evaluated by using energy dispersive spectral mapping**.** Spectrum confirms the presence of nickel and oxygen in pristine NiO and nickel, cerium and oxygen in $Ni_{0.99}Ce_{0.01}O$. Hence the presence of constituent elements is confirmed. Absence of foreign elements shows the phase integrity of the nano-sized structures[24]. The weight percentages of the elements are given in Table 3.3. The presence of carbon in the FE-SEM and EDAX spectra are due to the usage of carbon tape for measurements.

Table 3.3.The weight percentages of the elements

	$Ni_{0.99}Ce_{0.01}O$	**NiO**
Element	**Weight %**	**Weight %**
C K	**9.29**	**2.38**

O K	**10.11**	**9.11**
Ni K	**79.41**	**88.50**
Ce L	**1.19**	

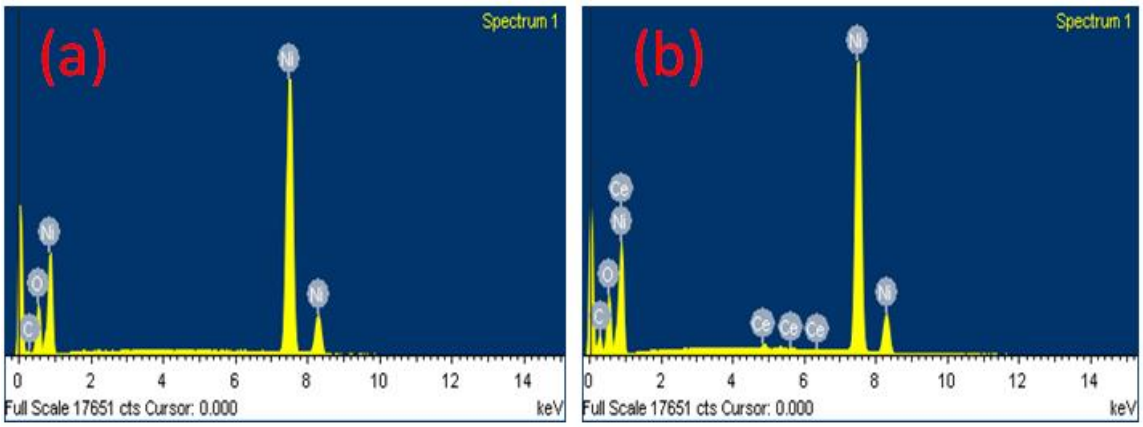

Fig. 3.5: **EDAX spectra of NiO and $Ni_{0.99}Ce_{0.01}O$**

RAMAN

Fig. 3.5 represents the Raman spectra of the prepared nanoparticles in the range 100-1400 cm^{-1}. The peak observed at 511 cm^{-1} is assigned to one-phonon (1P) mode of longitudinal optical (LO) NiO. The peak ascribed at 723 cm^{-1} corresponds to two-phonon (2P) modes of 2TO NiO whereas peak positioned at 1086 cm-1 represents to two-phonon 2LO mode respectively.

Doping with Ce leads to a shift in vibrational modes of NiO towards higher wavenumber region. Also, it is evident that, the peak intensity of Ce doped NiO nanomaterials is increased which is ascribed to defects in lattice vibrations due to oxygen vacancies. Meanwhile, it confirms the incorporation of Ce^{3+} ions in NiO lattice[25].

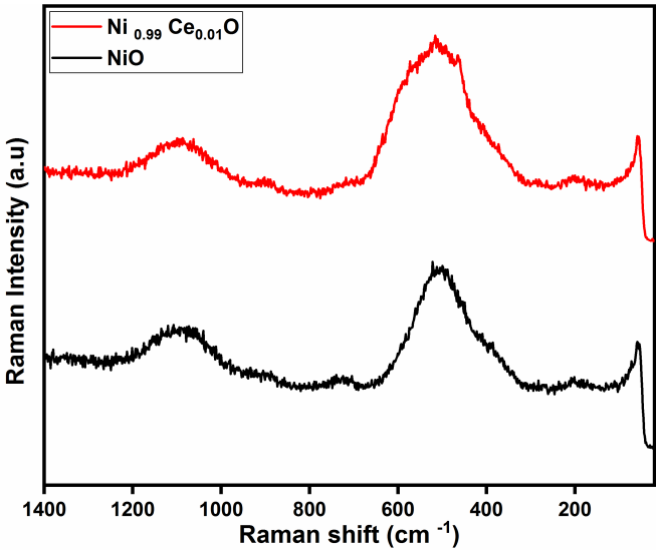

Fig. 3.6: **Raman spectra of NiO and $Ni_{0.99}Ce_{0.01}O$**

FTIR

The FTIR analysis of pure and Ce doped NiO nanoparticles was examined in the range of 400-4000 cm^{-1} and is shown in Fig. 3.6. All the samples exhibited a strong absorption peak at around 400 to 600 cm^{-1} which was ascribed to the presence of NiO nanoparticle vibration. Peak positioned at 453 cm^{-1} corresponds to Ni-O vibration of face-centered cubic crystal structure. The presence of two broad peaks at 1630 cm^{-1} and 3440 cm^{-1} corresponds to the bending and stretching modes of hydroxyl groups present in the water molecules. The peak appeared at 2358 cm-1 is due to CO2 species absorbed from the atmosphere [25].

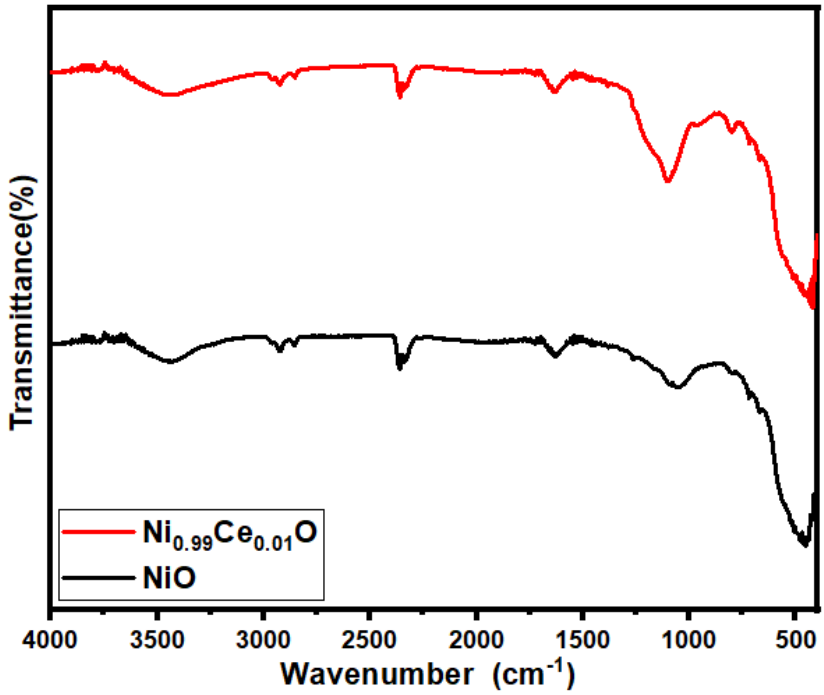

Fig.3.7: FTIR spectra of NiO and $Ni_{0.99}Ce_{0.01}O$

UV-Visible Absorbance

Linear optical behaviour of synthesized pristine and doped nanostructures can be identified from the UV-Visible absorbance spectrum, from which the classification of electronic transition along with bandgap energy can be evaluated. Whenever a semiconductor absorbs incident energy greater than its bandgap energy (E_g), the electron from its valence band will shift towards the conduction band and this causes an abrupt increase in the absorbance. Generally the type of transition depends on absorption coefficient (α) and photon energy. If the momentum of electron is conserved for a transition, then it is said to be as direct transition and on the other hand if the momentum of electron is not conserved, then it is called as indirect transition. Fig. 3.7 shows the absorbance spectra of NiO and $Ni_{0.99}Ce_{0.01}O$ in the range 200-800 nm. A strong absorption is observed in the range 200-400 nm. It is attributed to exciton transition.

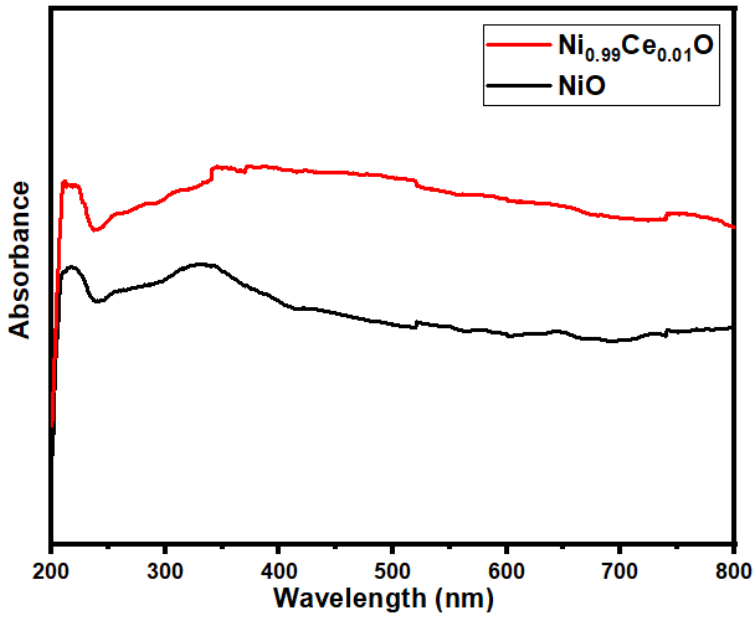

Fig.3.8: **Absorbance spectra of NiO and $Ni_{0.99}Ce_{0.01}O$**

For direct band gap materials, like NiO, bandgap (E_g) are related by the Tauc relation:

$$(\alpha h\upsilon)^{1/n} = A(h\upsilon - E_g)$$

where $E_g$stands for the energy bandgap and n denotes the kind of optical transition, here it is ½[26].

The bandgap energy has been evaluated by plotting $(\alpha h\upsilon)1/2$ and photon energy along Y and X-axis respectively is given in Fig. 3.8. By extrapolating the linear section in Fig. 3.8, energy bandgap of pristine and doped nanoparticles can be calculated. From the bandgap calculations, it is found that the bandgap is increasing. The presence of dopants/chemical defects or surface oxygen vacancies in the bandgap leads to the variation in the bandgap.

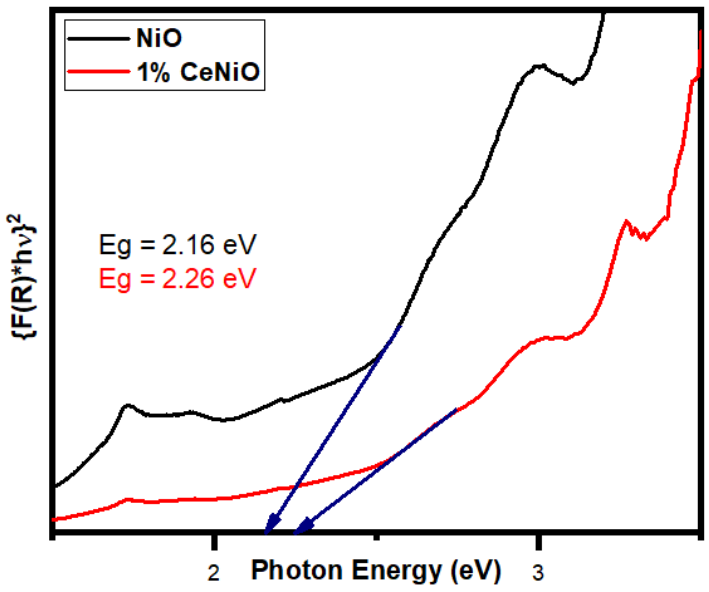

Fig.3. 9: **Bandgap determination of NiO and $Ni_{0.99}Ce_{0.01}O$**

Cyclic Voltammetry (CV) Analysis

Cyclic Voltammetry (CV) is used to distinguish the nature of the material. From the CV graph it is observed that the prepared samples exhibit EDLC behaviour. CV is performed with different scan rates. The specific capacitance was a maximum at lowest scan rates and decreased with increasing scan rates. In the case of electrical double-layer capacitance, the shape of the CV curve is normally close to that of a rectangle. The prepared samples showing a rectangular shape and thereby we can emphasize this material store charges by electrostatically. Nowadays, transition metal oxides are promising materials that are used in electrochemical applications. Cyclic voltammogram is recorded at different scan rates in the potential range of 0.0 to 0.7 V. The shape of CV curve indicates the EDLC behaviour of NiO electrodes. As the scan rate increases, the area of curves is also observed to be increased. After Ce doping also the shape of the CV image is not changed. From the CV image we can observe that after Ce doping the area of the curve is increased. When we compare the CV curve at scan rate of 20mv/S we can notice the distinguishable increase in the area of the prepared materials. Hence from CV analysis we can conclude that the capacitive performance is high for Ce doped NiO.

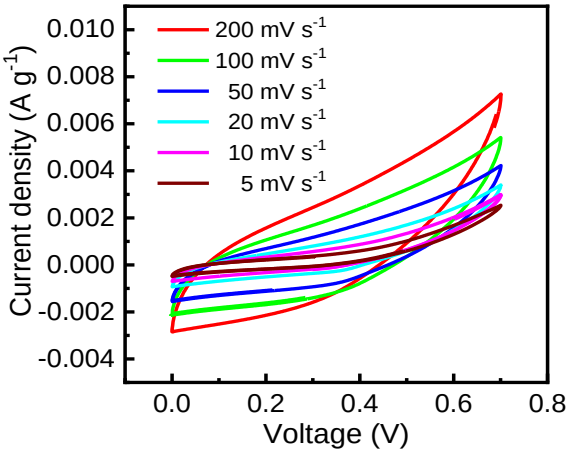

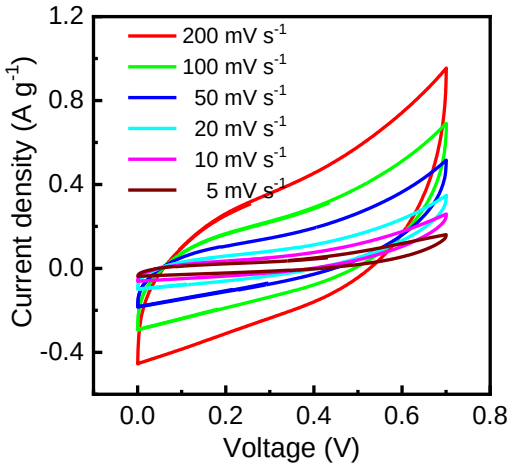

Fig4.0: CV image of pristine and Ce doped NiO

Galvanostatic Charge Discharge (GCD) Analysis

Charge discharge technique is used to calculate the specific capacitance of the material and it is more accurate inorder to calculate the capacitance. The linear curve of the sample is indicating that this material follows the EDLC behaviour. This is also validated from CV images also. Here also the GCD is recorded with different current densities. According to increase of current density the capacitance is decreased. The maximum capacitance is obtained in lowest current density. From the GCD curve itself we can observe that the discharging time is more at lowest current density. When we are comparing the discharging time of pristine and Ce doped NiO at current density 1A/g it showing more discharging time for doped sample. Potential window is taken 0.8V. The specific capacitance was calculated from the charge- discharge curve using the equation $C = \frac{i\Delta t}{m\Delta V}$, where i is the current density, m is the mass of the electroactive metal, ΔV is the potential window and Δt is the

discharge time. The highest capacitance is calculated for Ce doped NiO is about 4 F/g at current density of 1A/g. The capacitance for pristine is calculated as 1F/g.

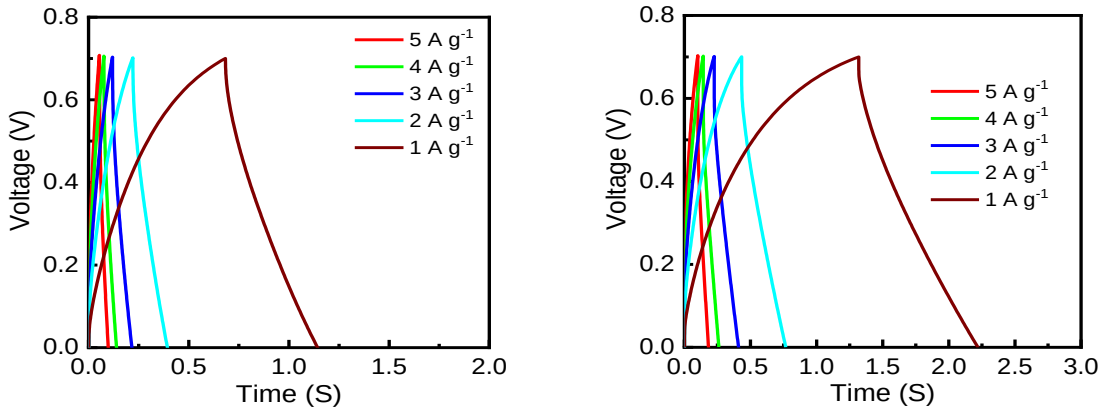

Fig4.1: GCD curve of pristine and Ce doped NiO

Electrochemical Impedance Spectroscopy (EIS)

EIS analyses were carried out to investigate the electrochemical impedance properties. We can analyse the resistance and conductivity of the material from EIS analysis. We plotted the nyquist plot by placing real part and imaginary resistance in X and Y axis respectively. By analysing the ohmic resistance or solution resistance it is very clear that the resistance value is less for doped sample compared to pristine. Solution resistance is the curve which intercept the point of X axis. This resistance is caused by the after effect of ion diffusion from electrode and electrolyte. The lowest resistance is observed for doped sample hence it will show the maximum conductivity. This result is validated from CV and GCD results.

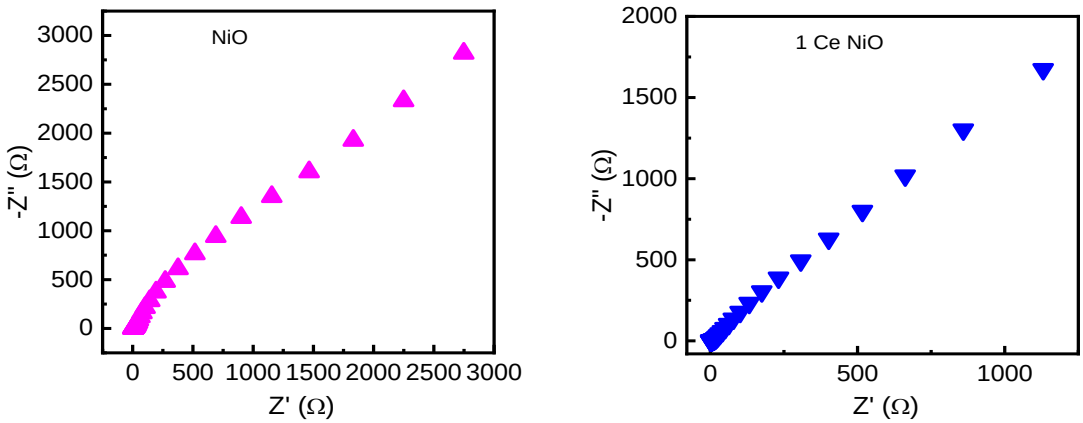

Fig4.2: EIS curve of Ce doped NiO and pristine samples

Chapter 4

Conclusions and Future scope

Conclusions

In the present work, modified auto combustion method is used to prepare pure and Ce doped NiO with controlled morphology. Using XRD, FE-SEM, EDAX, FTIR, and Raman spectroscopy, the structure, surface morphology, functional groups, and vibrational bands of NiO and Ce doped NiO have been examined. Using powder X-ray diffraction analysis, the phase purity and crystal structure of pure and Ce doped NiO nanostructures were examined. XRD analysis revealed the face-centered cubic structure with space group Fm-3m space group. No additional contaminant peaks were found within the experimental detection limit, and all of the diffraction peaks of the synthesised samples were ascribed to nickel oxide. This shows that the nickel oxide's lattice site has been doped with Ce without altering the crystal's symmetry. From the FE-SEM image, the morphology of the synthesised sample has been seen analysed. It is clearly observed that after doping no significant change in morphology happened. The presence of Ni, O and Ce were identified From EDAX spectra. Through FTIR, the functional groups of the produced sample are identified and are comparable to those of NiO. Raman spectroscopy is used to identify vibrational bands, which are the same as those described in published articles. Bandgap was determined using UV-visible spectroscopy and the value is in agreement with reported values.

Future scope

The current research investigation can be extended in the following directions:

- To analyse the effect of doping by studying higher doping concentrations.
- Inorder to understand more about the morphology of the prepared nanoparticles transmission electron microscopic (TEM) techniques can be used.
- Different electrolytes can be used inorder to obtain high density supercapacitor
- Supercapacitor device can be fabricated for large area with high mass loading to achieve high energy density and power density.

References

[1] Tomy Merin, Athira Ambika Rajappan, Vimuna VM, and Xavier Thankappan Suryabai. "Emergence of novel 2D materials for high-performance supercapacitor electrode applications: a brief review." Energy & Fuels 35, no. 24 (2021): 19881-19900.https://doi.org/10.1021/acs.energyfuels.1c02743

[2] M. Winter, R.J. Brodd, Chem. Rev, 104 (2004) 4245.

[3] Lokhande, Prasad Eknath, Chavan. "Synthesis and characterization of nanomaterial based supercapacitor for mechanical applications"(2020).http://hdl.handle.net/10603/216691.

[4] Sabatier, P. A. (1986).Top down and bottom up approaches to implementation research: a critical analysis and suggested synthesis. Journal of public policy, 6(1), 21-48.

[5] Klein, L; Aparicio, M.,& Jitianu, A. (Eds). (2016). Handbook of sol-gel science and technology. Springer International Publishing.

[6] Anjali, P.; Vani, R.; Sonia, T. S.; Nair, A. Sreekumaran; Ramakrishna, Seeram; Ranjusha, R.; Subramanian, K. R. V.; Sivakumar, N.; Mohan, C. Gopi; Nair, Shantikumar V.; Balakrishnan, Avinash (2014). Cerium Doped NiO Nanoparticles: A Novel Electrode Material for High Performance Pseudocapacitor Applications. Science of Advanced Materials, 6(1), 94–101. doi:10.1166/sam.2014.1684

[7] Gawali, Swati R.; Dubal, Deepak P.; Deonikar, Virendrakumar G.; Patil, Santosh S.; Patil, Seema D.; Gomez-Romero, Pedro; Patil, Deepak R.; Pant, Jayashree (2016). Asymmetric Supercapacitor Based on Nanostructured Ce-doped NiO (Ce: NiO) as Positive and Reduced Graphene Oxide (rGO) as Negative Electrode. ChemistrySelect, 1(13), 3471–3478. doi:10.1002/slct.201600566

[8] Isacfranklin, M.; Ravi, G.; Yuvakkumar, R.; Kumar, P.; Velauthapillai, Dhayalan; Saravanakumar, B.; Babu, E. Sunil (2020). AIP Conference Proceedings [AIP Publishing proceedings of advanced material, engineering & technology - Seoul, South Korea (29â€ "30 November 2019)] - proceedings of advanced material, engineering & technology Cerium doped NiO nanoparticles by hydrothermal method. , 2291(), 110022–. doi:10.1063/5.0019376

[9] PE, SARANYA; Selladurai, S (2019). Mesoporous 3D network Ce doped NiO nanoflakes as high performance electrodes for supercapacitor applications. New Journal of Chemistry, (), 10.1039.C9NJ00097F–. doi:10.1039/C9NJ00097F

[10] Dhas, S.D.; Maldar, P.S.; Patil, M.D.; Nagare, A.B.; Waikar, M.R.; Sonkawade, R.G.; Moholkar, A.V. (2020). Synthesis of NiO nanoparticles for supercapacitor application as an efficient electrode material. Vacuum, (), 109646–. doi:10.1016/j.vacuum.2020.109646

[11] Abdur Rahman, M., Radhakrishnan, R. Microstructural properties and antibacterial activity of Ce doped NiO through chemical method. SN Appl. Sci. **1**, 221 (2019).doi.org/10.1007/s42452-019-0232-y

[12] Gawali, Swati R.; Patil, Vithoba L.; Deonikar, Virendrakumar G.; Patil, Santosh S.; Patil, Deepak R.; Patil, Pramod S.; Pant, Jayashree (2017). Ce doped NiO nanoparticles as selective NO 2 gas sensor. Journal of Physics and Chemistry of Solids, (), S0022369717304912–. doi:10.1016/j.jpcs.2017.11.005

[13] Siddique, M. N., Ahmed, A., Riyajuddin, S. K., Faizan, M., Ghosh, K., & Tripathi, P. (2020). Exploring the Ce3+ ions doping effect on optical and magnetic properties of NiO nanostructures. Journal of magnetism and magnetic materials, *500*, 166323.

[14] Muthukumaran, P., Raju, C. V., Sumathi, C., Ravi, G., Solairaj, D., Rameshthangam, P. & Alwarappan, S. (2016). Cerium doped nickel-oxide nanostructures for riboflavin biosensing and antibacterial applications. New Journal of Chemistry, *40*(3), 2741-2748.

[15] Zhu, Ling; Zeng, Wen; Yang, Jingdong; Li, Yanqiong (2019). Unique hierarchical Ce-doped NiO microflowers with enhanced gas sensing performance. Materials Letters, 251(), 61–64. doi:10.1016/j.matlet.2019.05.055

[16] Dzakaria, N., Lahuri, A. H., Saharuddin, T. S. T., Samsuri, A., Salleh, F., Isahak, W. N. R. W. & Yarmo, M. A. (2021). Preparation of Cerium doped Nickel oxide for lower reduction temperature in carbon monoxide atmosphere. Malaysian Journal of Analytical Sciences, *25*(3), 521-531.

[17] Barbara, L.D Louisiana state university, Christine M. Clark, Eastern Michigan University. X-ray powder diffraction geochemical instrumentation and analysis.

[18] https:/en.wikipedia.org/wiki/scanning electron microscope

[19] O. Faix, Fourier Transform Infrared Spectroscopy, in: D.C.W. Lin S.Y. (Ed.), Methods Lignin Chem., Springer Berlin Heidelberg, 1992: pp. 83–109. doi:10.1007/978-3-642-74065-7_7.

[20] N. Elgrishi, K.J. Rountree, B.D. McCarthy, E.S. Rountree, T.T. Eisenhart, J.L. Dempsey, A Practical Beginner's Guide to Cyclic Voltammetry, J. Chem. Educ. 95 (2018) 197–206. doi:10.1021/acs.jchemed.7b00361.

[21] A. Manuscript, rsc.li/njc, (2019). Doi.org/10.1039/C9NJ00097F

[22] L. Zhu, W. Zeng, J. Yang, Y. Li, Unique hierarchical Ce-doped NiO microflowers with enhanced gas sensing performance, Mater. Lett. 251 (2019) 61–64. Doi.org/10.1016/i.matlet2019.05.0555

[23] S.R. Gawali, V.L. Patil, V.G. Deonikar, S.S. Patil, D.R. Patil, P.S. Patil, J. Pant, Journal of Physics and Chemistry of Solids Ce doped NiO nanoparticles as selective NO 2 gas sensor, J. Phys. Chem. Solids. 114 (2018) 28–35. Doi.org/10.1016/i.ipcs.2017.11.005

[24] M.A.R.R. Radhakrishnan, Microstructural properties and antibacterial activity of Ce doped NiO through chemical method, SN Appl. Sci. 1 (2019) 1–9. Doi.org/10.1007/s42452-019-0232-y

[25] S. Nair, Cerium Doped NiO Nanoparticles : A Novel Electrode Material for High Performance Pseudocapacitor Applications Cerium Doped NiO Nanoparticles : A Novel Electrode Material for High Performance Pseudocapacitor Applications, (n.d.). Doi.org/10.1166/sam.2014.1684

[26] M.N. Siddique, A. Ahmed, S.K. Riyajuddin, M. Faizan, K. Ghosh, Journal of Magnetism and Magnetic Materials Exploring the Ce 3 + ions doping e ff ect on optical and magnetic properties of NiO nanostructures, J. Magn. Magn. Mater. 500 (2020) 166323. https://doi.org/10.1016/j.jmmm.2019.166323.